8808057

I

RAPPORT

Jürgen König

The Structural Behavior of Axially Loaded Wood Studs Exposed to Fire on One Side

Trätek

INSTITUTET FÖR TRÄTEKNISK FORSKNING

Jürgen König

THE STRUCTURAL BEHAVIOUR OF AXIALLY LOADED WOOD STUDS EXPOSED TO FIRE ON ONE SIDE

TräteknikCentrum, Rapport I 8808057

Nyckelord

buckling
fire resistance
load bearing capacity
structural behaviour
studs
walls
wood

Stockholm August 1988

Rapporter från TräteknikCentrum är kompletta sammanställningar av forskningsresultat eller översikter, utvecklingar och studier. Publicerade rapporter betecknas med I eller P och numreras tillsammans med alla utgåvor från TräteknikCentrum i löpande följd.

Rapporter kan som regel beställas kostnadsfritt i ett exemplar av medlemsföretag. Ytterligare beställda exemplar faktureras.

Citat tillåtes om källan anges.

Reports issued by the Swedish Institute for Wood Technology Research comprise complete accounts for research results, or summaries, surveys and studies. Published reports bear the designation I or P and are numbered in consecutive order together with all the other publications from the Institute.

Member companies may generally order one copy of any report free of charge. A charge will be made for any further copies ordered.

Extracts from the text may be reproduced provided the source is acknowledged.

TräteknikCentrum betjänar de fem industrigrenarna sågverk, trämanufaktur (snickeri-, trähus-, möbel- och övrig träbearbetande industri), träfiberskivor, spånskivor och plywood. Ett avtal om forskning och utveckling mellan industrin och Styrelsen för Teknisk Utveckling (STU) utgör grunden för verksamheten som utförs med egna, samverkande och externa resurser. TräteknikCentrum har forskningsenheter, förutom i Stockholm, även i Jönköping och Skellefteå.

The Swedish Institute for Wood Technology Research serves the five branches of the industry: sawmills, manufacturing (joinery, wooden houses, furniture and other woodworking plants), fibre board, particle board and plywood. A research and development agreement between the industry and the Swedish National Board for Technical Development (STU) forms the basis for the Institute's activities. The Institute utilises its own resources as well as those of its collaborators and other outside bodies. Apart from Stockholm, research units are also located in Jönköping and Skellefteå.

C O N T E N T S

		Page
FOREWORD		3
SUMMARY		4
1.	BACKGROUND AND AIMS	5
2.	EXPERIMENTAL INVESTIGATIONS	6
	2.1 General	6
	2.2 Specimens and test apparatus	7
	2.3 Test procedure and results	10
	2.4 Evaluation	24
	2.41 Bending stiffness	24
	2.42 Stresses at midsection at failure	25
3.	ANALYTICAL MODELS	27
	3.1 Member with pin jointed end supports in compression	27
	3.2 Member with cylindrical convex end surfaces in compression	29
	3.21 Critical load	29
	3.22 Eccentric compressive force	29
	3.23 Determination of the ideal radius of the studs and surfaces	30
	3.24 The influence of the stud cross section	36
	3.25 The influence of the length of the stud	37
	3.26 The influence of support inclination on loadbearing capacity	38
	3.27 Superposition of axial force and transverse loading	39
4.	CONCLUSIONS	41
REFERENCES		43
APPENDIX A1	Determination of the critical load for a member with cylindrical convex end surfaces	44
APPENDIX A2	Member with cylindrical convex end surfaces acted upon by eccentric compressive load	47
APPENDIX A3	The influence of inclined support plates on a member with cylindrical convex end surfaces acted upon by a compressive force	51
APPENDIX A4	Eccentric axial force and transverse load on a member with cylindrical convex end surfaces	52
APPENDIX A5	Member with initial curvature and cylindrical convex end surfaces acted upon by a compressive force	54

FOREWORD

The investigations described in this report were initiated by the wish of the representatives of industry to improve present methods for the design with respect to fire of walls for single family houses. The original plan had been that the problem would be studied only experimentally. However, during evaluation of the experiments a number of phenomena arose which necessitated elucidation by means of theoretical studies. I wish to thank Birgit Östman for her support in carrying out this work.

The tests were made by Claes Kullberg at the Department of Steel Construction, Royal Institute of Technology, Stockholm. Joakim Norén assisted in the tests and evaluation. Bo Källsner provided valuable and critical observations.

The figures were drawn by Pi Dragojevic, and the manuscript was typed by Yvonne Larsson.

The work was financed by funds from the timber industry and the Swedish Board for Technical Development (STU) to the Swedish Institute for Wood Technology Research.

The Swedish original was translated by L J Gruber BSc(Eng) MICE MIStructE.

In this edition subsection 3.24 was shortened and a new appendix A5 was supplemented.

I wish to extend my sincere thanks to all who have contributed to this work.

Stockholm, August 1988

Jürgen König

SUMMARY

In Sweden, the loadbearing walls of single family houses must at present be designed with respect to fire in order to provide the necessary degree of safety against the spread of fire. One of the preconditions in order that the fire resistance of an external wall should be secured is that its loadbearing capacity should be maintained.

With the aim of studying the structural behaviour of wood studs, a test series was carried out on axially loaded wood studs. In these tests, the effect of fire on the wood studs was simulated by removing layers from the stud by planing it on the side which was supposed to be exposed to fire. Different support conditions, such as the use of cellular rubber sole plate sealing strips and inclined base or inclined roof truss rafter, were studied. Six of the specimens consisted of solid 45 x 120 mm timber studs, and two were lightweight studs comprising timber flanges and webs of wood fibre board. In all cases the studs were joined by short pieces of timber corresponding to the sole plate and top plate. During the tests, the specimens were placed between rigid, non rotating support plates, the intention being to reproduce conditions in a single family house construction.

In the theoretical part of the investigation, two analytical models are studied. In one of the models it is assumed that the ends of the stud are pinjointed. The structural behaviour cannot be described satisfactorily by this model. In the other analytical model, the stud is assumed to be placed between rigid end plates as in the tests. The end surfaces of the stud are idealised as cylindrical convex surfaces, enabling a rolling motion to take place as loading and deformations proceed. Theoretical solutions are derived for different loading cases and boundary conditions. In order that it should be possible to apply these, ideal radii are determined with the aid of the test results to describe the geometrical shape of the end surfaces. An approximate expression for the ideal radius is formulated in order that it may also be used for other cross sections and lengths.

With the aid of parametric studies, the influence due to inclination of the base and the interaction between axial force and transverse load is studied. The results show that the two load components can be superimposed by applying linear interaction.

Fire tests can thus be carried out separately for axial and transverse loading. By determining the loadbearing capacity for a certain fire resistance period, it will be possible to design a timber stud under fire exposure conditions for arbitrary loads and load combinations.

1. BACKGROUND AND AIMS

Design of the structural elements in a building with respect to fire is today an obvious part of overall design. In order that the required degree of safety against the spread of fire may be provided, it is essential that, in particular, the external walls of houses should have adequate fire resistance.

The fire resistance of a wall is its ability to function as a barrier against fire. In the case of walls which have only a space separating function, fire resistance depends on the insulation of the wall to limit the flow of heat through the wall, and also on its integrity to prevent passage of flames or hot gases. In the case of loadbearing walls, fire resistance is in addition limited by the ability of the wall to carry the imposed loads.

For the loadbearing external walls of single family houses and similar buildings, loading consists of an axial and a transverse load. These loads are due, for instance, to dead load, snow load on the roof, imposed loads on the attic storey, and wind loads on the walls.

As a rule, the load on a wall varies from case to case. The snow loads on the roof and the wind loads depend on where in the country the building is situated, and the imposed loads depend on the type of building in question. It is therefore desirable that design of walls for the loading case fire should be carried out in such a way that the actual loads and different combinations of these can be taken into consideration. A design method must also facilitate the application of different partial coefficients, which is important in conjunction with the export of prefabricated houses.

As a rule, the fire resistance of lightweight wall constructions such as timber stud walls is today determined in Sweden by fire tests at full scale. In order to simplify testing, the wall is generally acted upon only by axial loads which are however, in order to take account of the action of transverse forces, applied with a certain eccentricity. The supports of the wall are pin jointed /1/.

In a number of cases, this procedure results in considerable underestimation of the loadbearing capacity of the construction, since the structural behaviour of an actual construction is not reproduced in the correct way.

The aim of the experimental part of the investigation described in this report was to study the structural behaviour of the studs. The fire and its effects, charring and the thermal effects on the strength and stiffness of the remaining cross section, were simulated qualitatively by planing the studs on the side exposed to fire.

The aim of the theoretical part of the investigation was to provide an explanation for all the phenomena observed in the tests, and to have the capability to deal also with other types of loads and load combinations and thus to minimise the number of tests.

The thermal effects on strength and stiffness did not come within the terms of reference of this investigation. It is important that these should be studied separately so that the results can be used in a theoretical treatment of the problem, and the number of fire tests can be reduced.

2. EXPERIMENTAL INVESTIGATIONS

2.1 General

In many cases, the framing in the loadbearing external walls for single family houses today consists of solid vertical studs and horizontal studs attached to the outside faces of these. The cladding on the outside acts as wind protection and, when there are no horizontal studs, also has the function of preventing buckling of the studs in the plane of the wall. At present, common stud dimensions are 45 x 120 mm and 45 x 170 mm. In most cases, these studs are within the classification "Ö-virke" according to Swedish Building Code SBN 1980 /2/. Walls comprising lightweight studs, which may be composite I-sections consisting of flanges of small dimension timber and a web of wood fibre board, are becoming increasingly common. In these walls the cladding which provides protection against the wind is attached directly to the external flanges of the lightweight studs. The walls are filled with mineral wool in order to provide satisfactory thermal insulation.

In the event of fire, the internal board lining provides the initial barrier. After some time this burns completely or falls down from the wall, see e.g. /3/ (Noren and Östman, 1985). The loadbearing vertical studs are then directly exposed to fire. Since the mineral wool protects the sides of the studs from the fire, combustion takes place mainly on the inside of the wall. See Figure 2.1. The aim of the tests reported here was to study the mechanical deformation and failure behaviour of axially loaded cross sections exposed to fire on one side. For this reason, the fire sequence was simulated by successively removing a part of the cross section by planing, so that the effective cross section of the stud was gradually reduced. The rate of combustion is somewhat greater at the corners, and the boundary of the effective cross section is therefore a little rounded on the side towards the fire. However, this was not taken into account in the tests since the general behaviour of the specimens is not affected. The cross section of the studs and flanges was thus rectangular at all stages of the test.

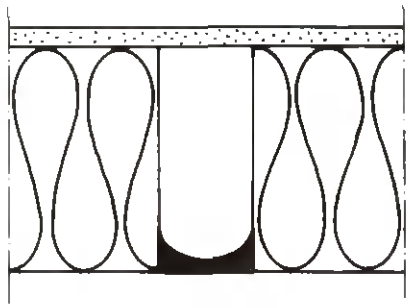

Figure 2.1.
Stage of fire after loss of the internal lining.

Since support conditions can vary considerably in practice, the effect of these on the behaviour of the studs was also studied in the tests. In order to ensure that buildings are airtight, sealing strips of cellular rubber are at present placed between the sole plate or top plate and adjoining parts of the building. Inclination of the foundation or deflection of the roof truss may have the effect that load is applied at a large eccentricity.

2.2 Specimens and test apparatus

Two types of specimen were investigated. Each specimen consisted of a stud of 2,400 mm length and pieces of timber 250 mm long and 45 mm thick which represented the sole plate and top plate in the actual construction.

The six specimens of Type 1 comprised solid timber studs of pine (Pinus sylvestris) in the Swedish grade Ö-virke (the characteristic bending strength is 15 N/mm^2), of the dimensions 45 x 120 mm. The timber for the sole plate and top plate had the same dimensions and was in the same grade. The nailed joints consisted of 2 No 100 x 3.4 nails driven straight through the sole plate and top plate into the end grain of the studs. Four of the specimens were fitted with cellular rubber sealing tapes (AB Värnamo Gummifabrik); these were attached to the sole plate and top plate by staples. See the summary in Table 2.1 and Figure 2.2. In the specimens where the sealing tape was narrower than the timber, it was placed centrally.

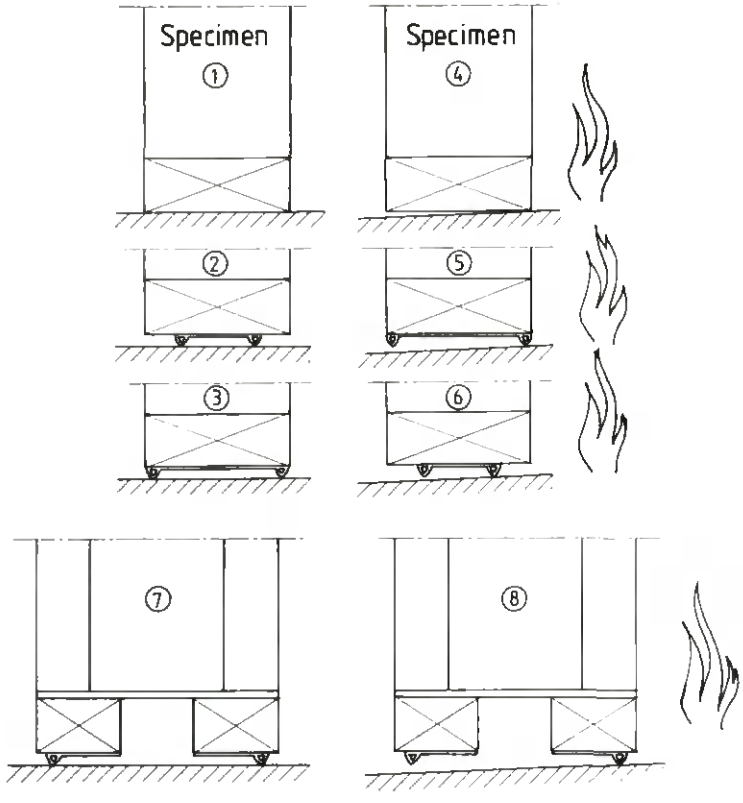

Figure 2.2. Support conditions in the tests. The upper support plate is horizontal in all tests.

Table 2.1. Design of specimens and supports in the tests with axial load.

Specimen	Stud	Sole plate/ top plate	Sealing strip	Inclination of bottom support plate (%)	Remarks
1	45 x 120	45 x 120	-	0	
2	45 x 120	45 x 120	70 x 10	0	
3	45 x 120	45 x 120	120 x 10	0	
4	45 x 120	45 x 120	-	3.5	
5	45 x 120	45 x 120	120 x 10	3.5	
6	45 x 120	45 x 120	70 x 10	3.5	
7	H 200 MB	H 200 MS	120 x 10[a)]	0	Lightweight stud
8	H 200 MB	H 200 MS	120 x 10[a)]	3.5	- " - b)

a) Cut and fitted as in Figure 2.2.
b) Splice in web 260 mm from bottom end of stud.

The two specimens of Type 2 consisted of Masonite Byggsystem lightweight studs made by Swanboard Masonite AB, of 2,400 mm length and stud depth 200 mm. The dimensions of the flanges were 45 x 45 mm and the thickness of the wood fibre board web 6.4 mm. All dimensions are nominal. The flanges were of spruce (Abies alba) and, according to information supplied by the manufacturer, were at least of grade T 18, while the grade of the web was at least K 13. No checks were made to find whether the specimens complied with these data. The sole plate and top plate consisted of 45 x 70 mm timber and the web of wood fibre board 8 mm thick. The minimum grades in this case also were the same as for the studs. The 120 x 10 mm sealing tape was cut in the middle and was attached to the sole plate and head plate at a distance of 10 mm from the end (Figure 2.2).

The testing machine for axial loading was a hydraulic press (Losenhausen) of 6,000 kN load capacity. It was fitted with rigid end plates which were prevented to rotate. For four of the specimens the lower support plate was inclined 3.5 % so that the undeformed specimen was in contact with the base on the "fire"-side.

The lower support plate was placed on three load cells (Alexen Load Indicator, capacity 50 kN) in order that the position of the axial force may be determined. See Figure 2.3. Using the symbols in the figure, this is determined as:

$$d = \frac{-aA - bB + cC}{N}$$

The dimensions a, b and c are set out in Table 2.2.

Buckling in the direction of the minor axis of the stud was prevented by means of lateral supports with sliding bearings of teflon strips, fitted at the midpoint and quarter points. For specimens Nos 7 and 8 (lightweight studs), only the outer flange (that unaffected by the "fire") was braced in such a way.

Displacement in the stiff direction of the stud was measured at midheight by means of a rotary potentiometer type transducer (Novotechnik) with an accuracy better than ± 0.025 mm.

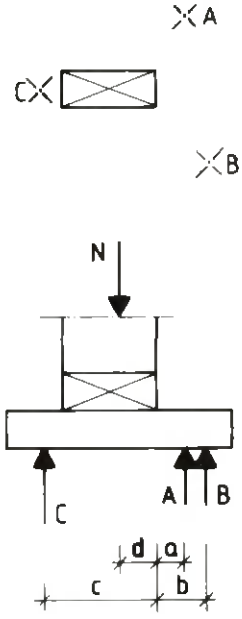

Figure 2.3.
Placing of load cells for determination of the position of the axial force.

Table 2.2. Placing of load cells.

Specimen	a mm	b mm	c mm
1 - 6	154	33,9	33,4
7, 8	240	0	0

On all specimens, a transverse load was also applied in the stiff direction in order that flexural rigidity may be determined, see Figure 2.4. When the compression flange had been removed from specimens Nos. 7 and 8, the load was transmitted to the tension flange by means of blocks of wood on each side of the web. Load was applied by a hydraulic jack and measured with a load cell. The measured load values had the accuracy ± 20 N.

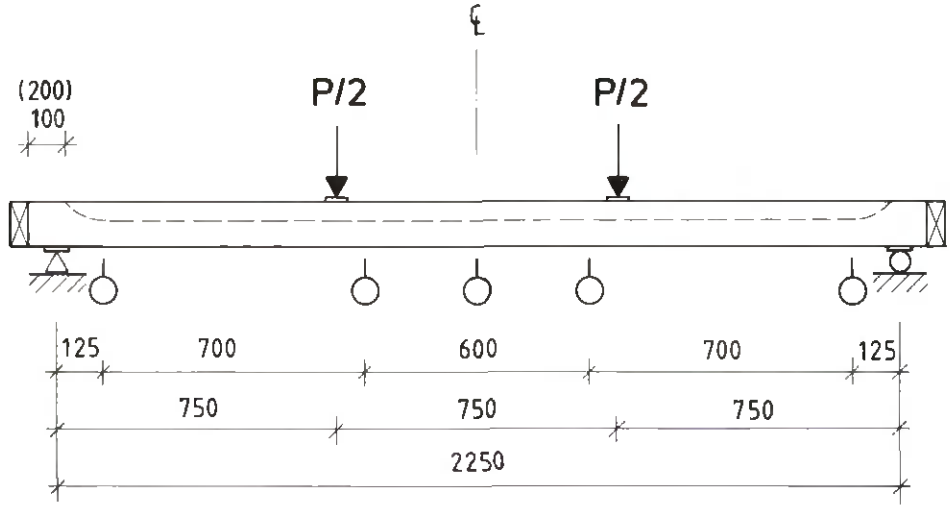

Figure 2.4. System and loading for determination of flexural rigidity.

2.3 Test procedure and results

The specimens were conditioned in a controlled climate room at 20 °C and 65 % RH for about one week. Testing commenced even if there was no certainty that the equilibrium moisture ratio had been attained. The reason for this was that it was primarily the behaviour at failure which was to be studied. The ultimate load of axially loaded studs of large slenderness ratio is mainly governed by flexural rigidity, see the formula for the Euler load. Since the influence of the moisture ratio on flexural rigidity is substantially less than on the strength, deviations from the equilibrium moisture ratio can be ignored. The moisture ratio and dry density were determined on samples taken from the timber near the position of fracture, and are set out in Table 2.3.

Table 2.3. Type of timber, moisture ratio and dry density of specimens.

Specimen	Timber	Moisture ratio u %	Dry density ϱ_{ou} kg/m^3
1	Pine	14.2	449
2	"	14.4	393
3	"	14.6	424
4	"	14.2	422
5	"	13.8	384
6	"	13.9	437
7	Spruce	14.0	369
8	"	14.1	355

The specimens were first tested under transverse load and then under axial load. After this a layer of the material was removed on the side of the stud exposed to fire with a jig saw and electric plane. For specimen 1 reduction of the cross section began 200 mm from the ends of the stud, for other specimens reduction began 100 mm from the ends of the stud, see Figure 2.4. The material was planed in steps of 5 mm on Specimen No. 1 and in steps of 10 mm on the other specimens. Deviations from this, at the final stage near failure, are set out in Table 2.4. Reduction of the cross section in Specimens Nos. 7 and 8 (lightweight studs) was as shown in Figure 2.5.

Table 2.4. Results for the ultimate stage.

Specimen	Depth of cross section at failure h mm	Depth of cross section prior to failure[a] h mm	Maximum load N_{max} kN	Ultimate load N_u kN	Time	Distance of N_u from edge d mm
1	55	60	13.0	12.80	0	18.8
2	50	60	13.0	9.22	0	15.2
3	55	60	13.0	12.36	0	17.9
4	60	60	13.0	13.00	2 h, 4 min	10.3[c]
5	55	55	13.0	13.00	8 min	19.0[c]
6	54.5	60	13.0	11.07	0	17.7
7	85	110	18.0	12.92	0	15.4
8	135	160[b]	18.0	17.81	0	23.7

a) This cross section maintained the maximum load for at least 5 minutes.
b) Without flange.
c) At the end of the creep stage, see Figure 2.13.

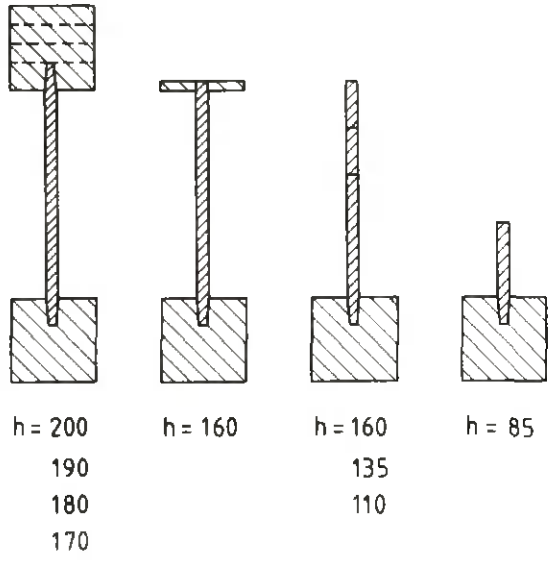

Figure 2.5. Stages of cross section for specimens Nos. 7 and 8.

During the tests under transverse load according to Figure 2.4, the load and deflection were recorded for integral values of the midpoint deflection until this was 5 mm, whereupon the specimen was immediately unloaded. The rate of loading was such that application of load proceeded for at least 2 minutes. An example of the measured relationship between load and midpoint deflection is shown in Figure 2.6.

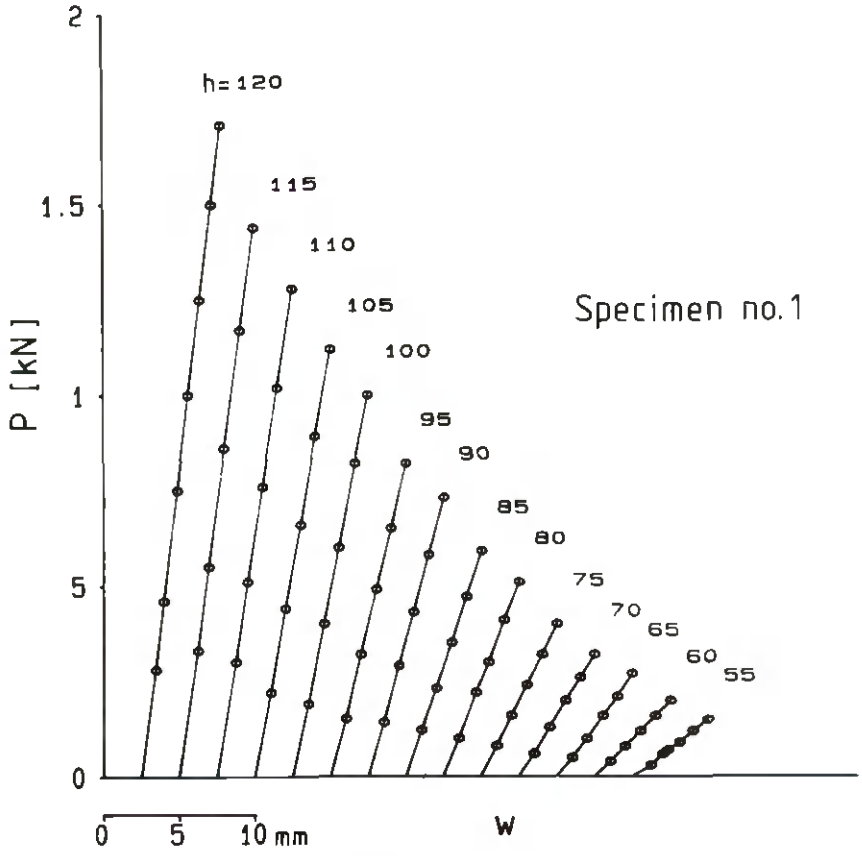

Figure 2.6. Examples of transverse load - midpoint deflection curves for different depths of the cross section.

The specimens were then placed in the test apparatus for axial loading. Load was applied at a constant rate until the maximum load of 13 kN and 18 kN respectively was attained after about 4 minutes. The readings from the load cells and displacement transducers were recorded for each loading stage of 1 kN. When the maximum load had been reached, it was maintained constant for 5 minutes and the readings were recorded after every minute. The specimen was then immediately unloaded.

The maximum load chosen was a little less than that permitted according to Swedish Building Code SBN 1980 /2/. This was calculated with respect to buckling in the stiff direction for specimens of Type 1 and had the magnitude 13.7 kN. For these specimens, the permissible load with respect to compression perpendicular to the grain is 10.8 kN, which was thus exceeded in the tests. For specimens of Type 2, i.e. the lightweight beams, the permissible axial load is 18.8 kN according to data supplied by the manufactu-

rer. In this case the design criterion is compression perpendicular to the grain in the sole plate and top plate respectively.

In most of the specimens failure occurred already before the whole of the axial load had been applied. In two of the specimens, however, where the maximum load was kept constant for 5 minutes, it was evident that the specimen would creep to failure even without further reduction of the cross section. In specimen No. 4 this creep process took over 2 hours. The values of the ultimate loads N_u, depth of cross section h at failure and a stage of the cross section before failure, and the time over which the maximum load N_u was maintained, are set out in Table 2.4.

Axial load - midpoint deflection curves are given in Figure 2.7 a-g. The results for specimen No. 8 are not given. The reason for this is that the presence of a butt joint in the web near the bottom support had such an effect on the deflected shape that the maximum deflection did not occur at the centre. See below. In order to illustrate the influence of the different boundary conditions on the deformations in specimens Nos. 1-6, the curves for the least cross sections of the specimens are also given separately in Figure 2.8. On comparing the reasonably straight portions of the curves as load began to be applied, it is seen that the smallest displacements occurred in specimens Nos. 1 and 4 which were not fitted with sealing strips. Specimens Nos. 3 and 5, with 120 mm wide sealing strips, come next. The largest displacements occurred in specimens Nos. 2 and 6 which were fitted with 70 mm wide strips. In all three pairs of specimens, the largest displacement was recorded for the specimen which had an inclined support plate.

Figure 2.7 a-g. Axial force - midpoint deflection curves for different depths of the cross section.

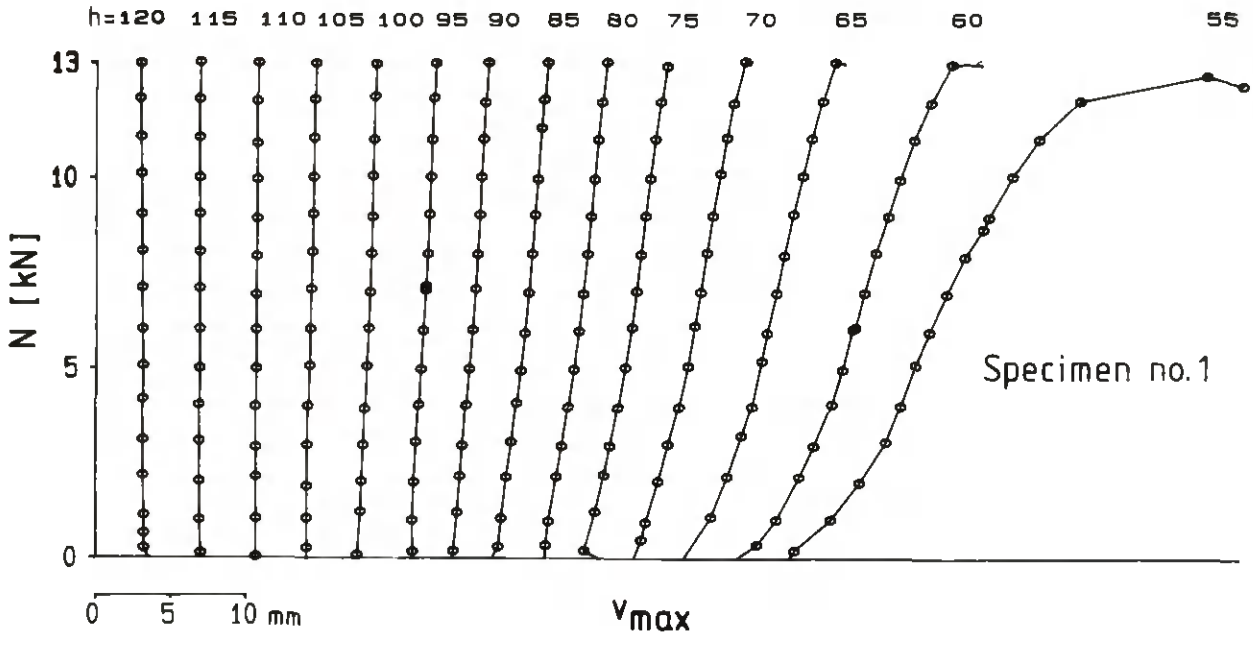

Figure 2.7 a.

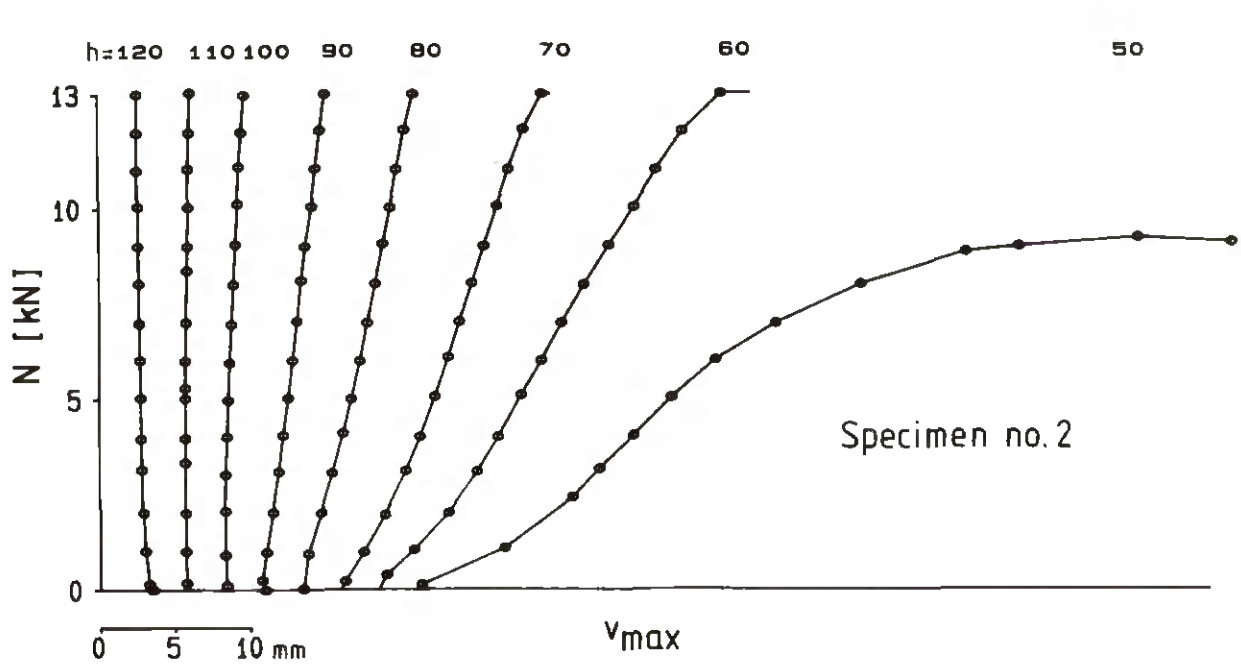

Figure 2.7 b.

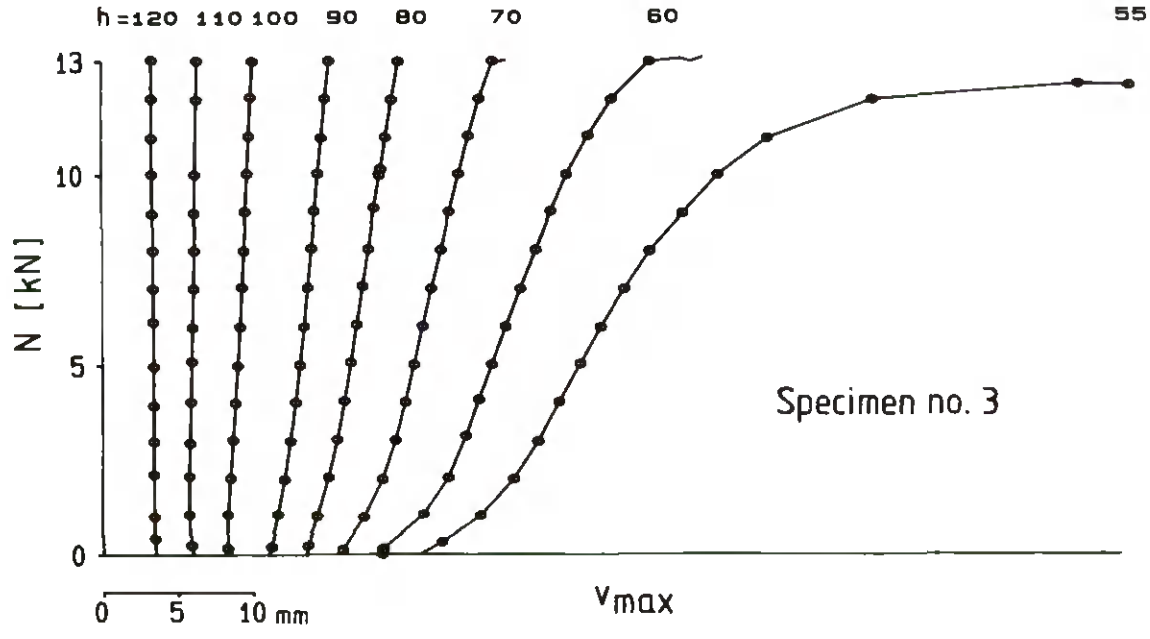

Figure 2.7 c.

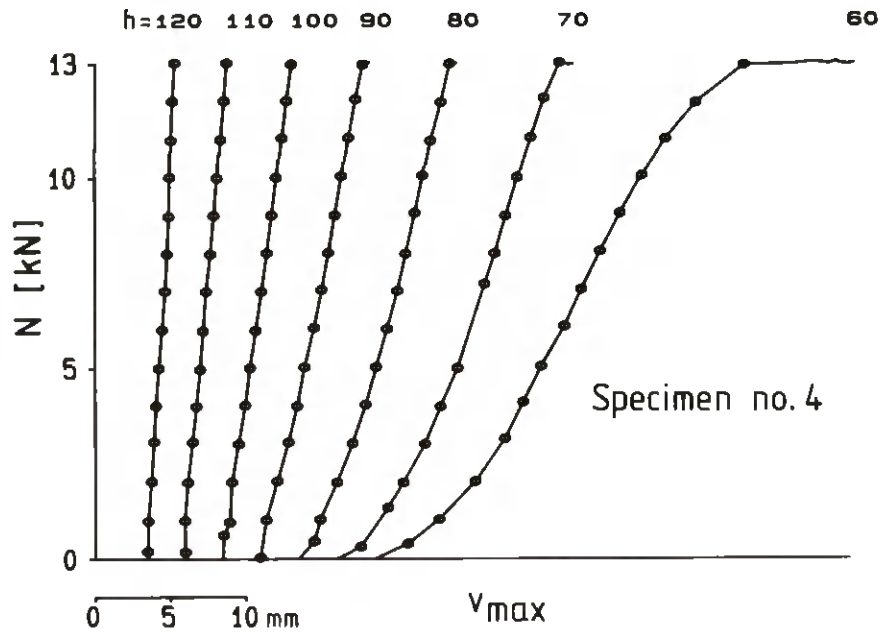

Figure 2.7 d.

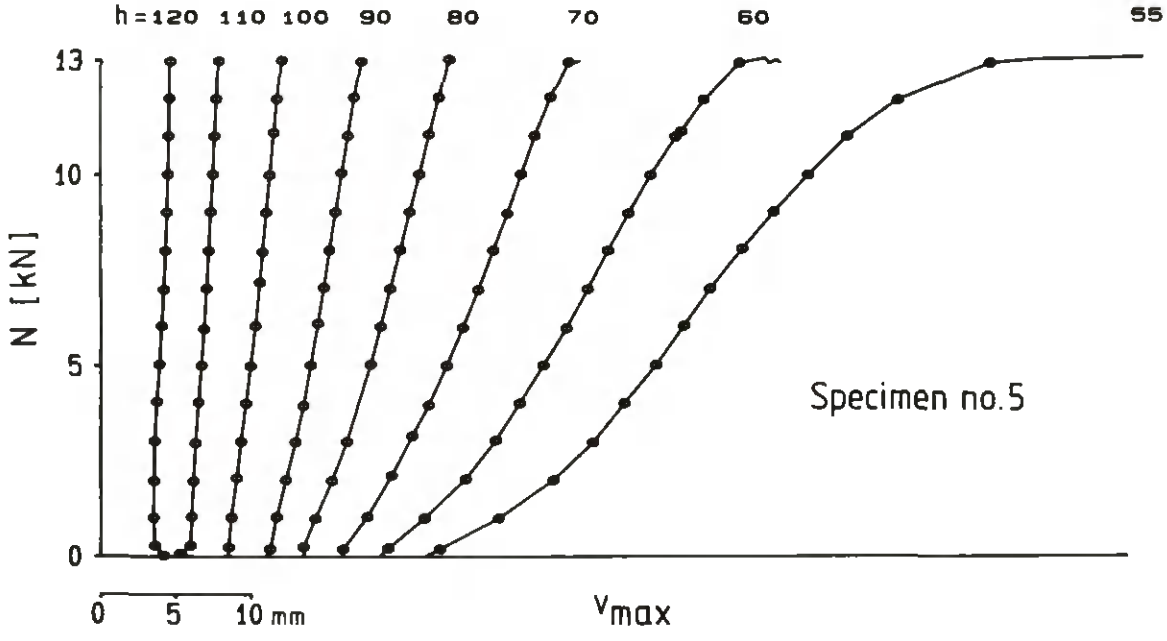

Figure 2.7 e.

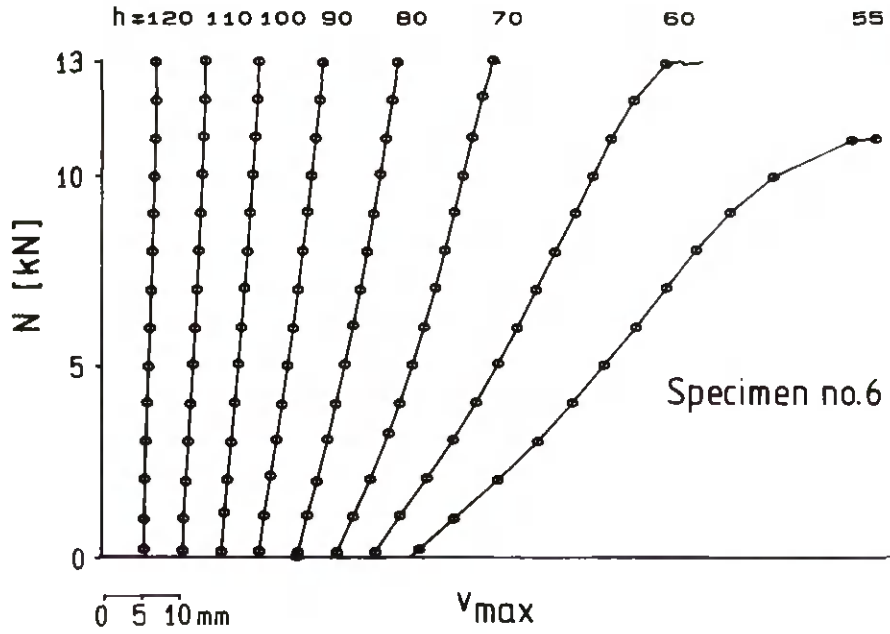

Figure 2.7 f.

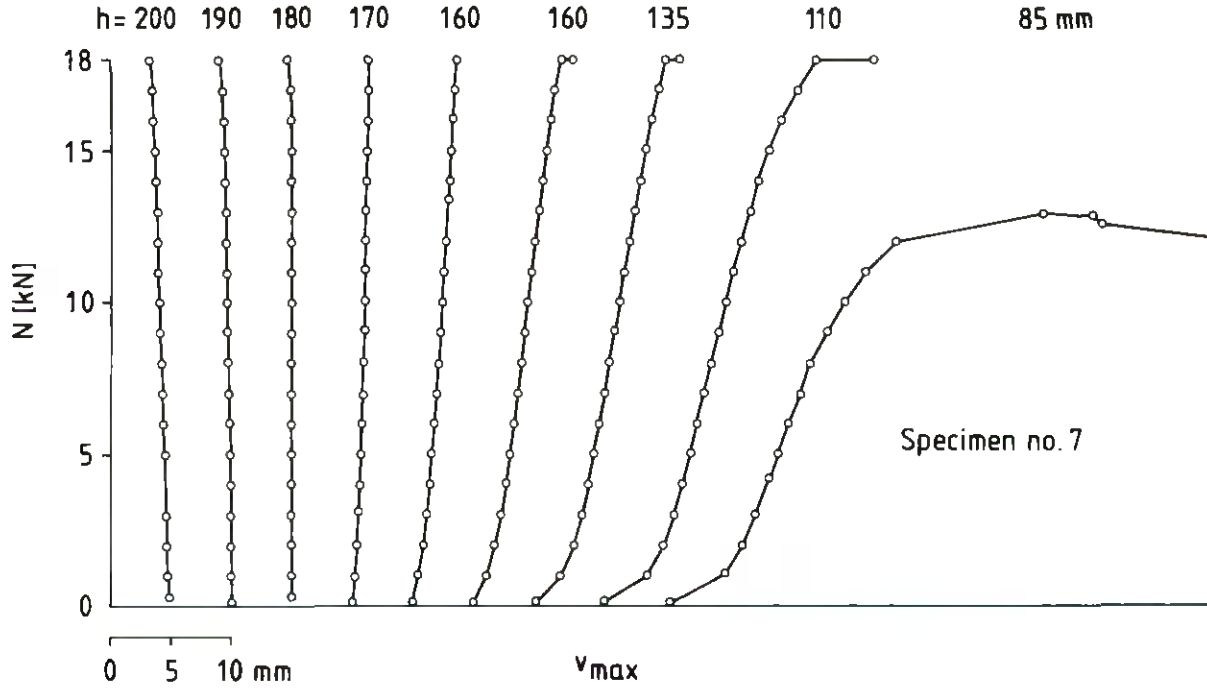

Figure 2.7 g.

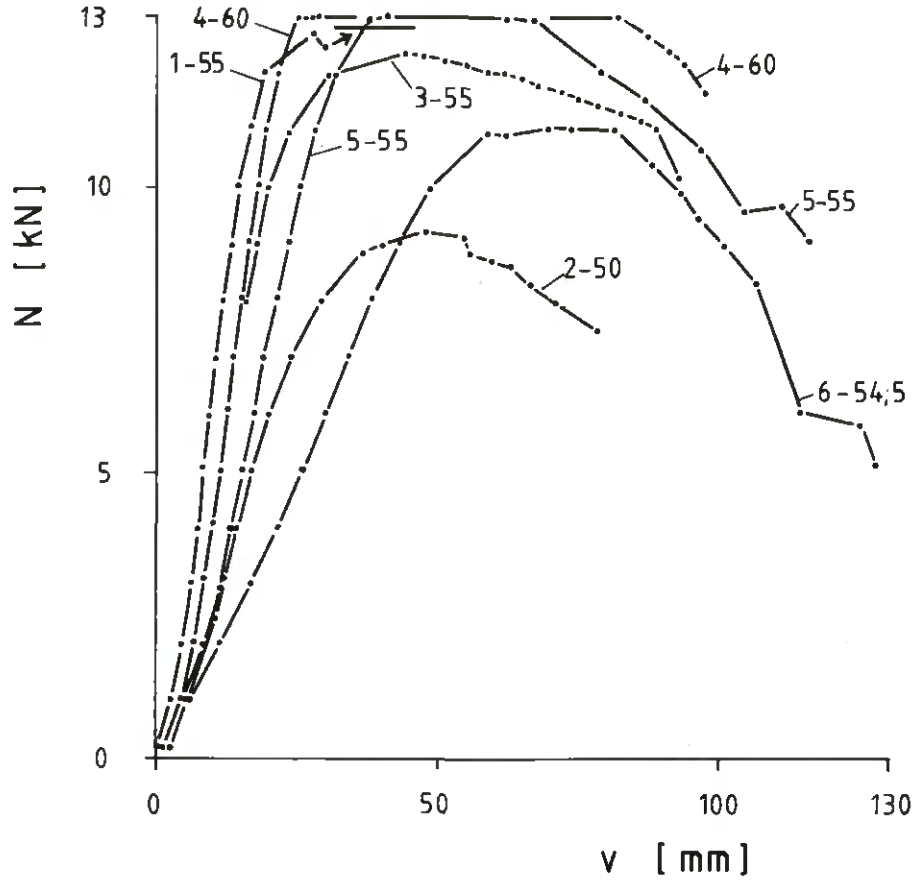

Figure 2.8. Axial force - midpoint deflection curves for the smallest cross sections of specimens Nos 1-6.

As load was increased, it was noted that the ends of the studs rotated so that contact with the base plate was concentrated increasingly towards the outer edge of the stud, while on the opposite edge a gap opened between stud and sole plate and between sole plate and base plate. See Figure 2.9 and 2.10. Near failure, this gap extended right up to the middle of the cross section. It is quite evident that the position of the axial load was displaced during the test towards the outer edge of the stud.

The general state of affairs regarding the position of the axial force and the deflection of the stud is set out in Figure 2.11. In Figure 2.12, the position of the axial force and the geometrical centre of gravity in the centre is shown with full curves for the maximum axial load for the different stages of the cross section. The stages where the maximum load had not been reached are marked with dashed curves. The distance between the two curves in the diagrams represents the lever arm of the bending moment in the centre.

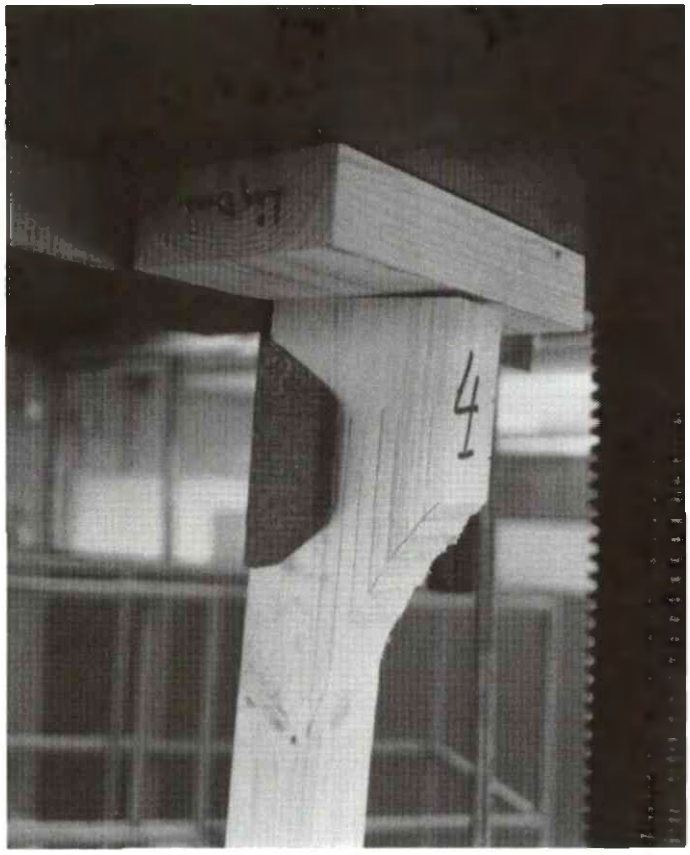

Figure 2.9.
Deformations at the upper horizontal support in specimen No. 4-60 at maximum load.

Figure 2.10.
Deformations at the bottom inclined support in specimen No. 4-60 at maximum load.

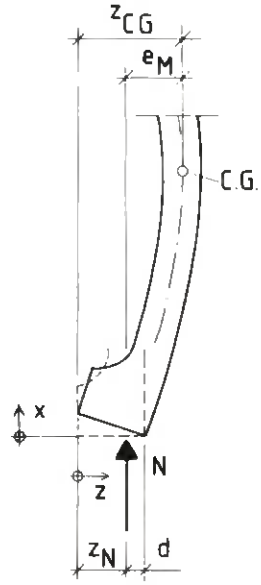

Figure 2.11.
Positions of the axial force x_N and the geometrical centre of gravity x_{CG} for the midsection in the deflected position.

Figure 2.12 a-h. The position of the axial force x_N at the bottom support of the stud and the position of the geometrical centre of gravity x_{CG} in the centre. Except for the dashed portions where the maximum load had not been reached, the curves relate to the maximum axial force.

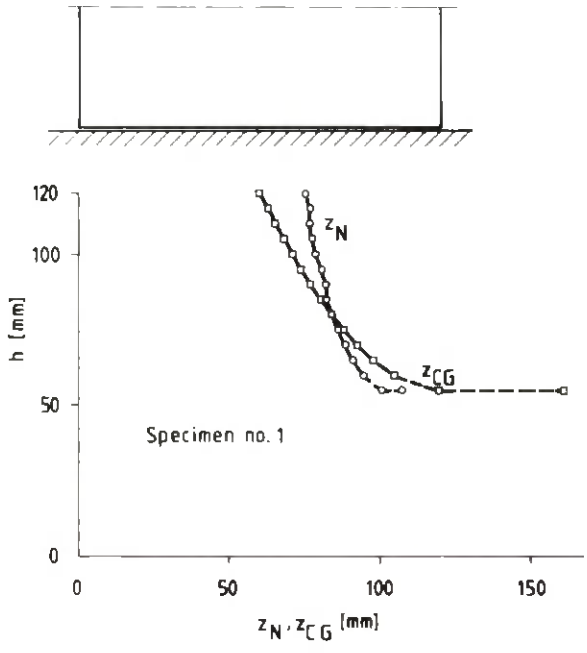

Figure 2.12 a.

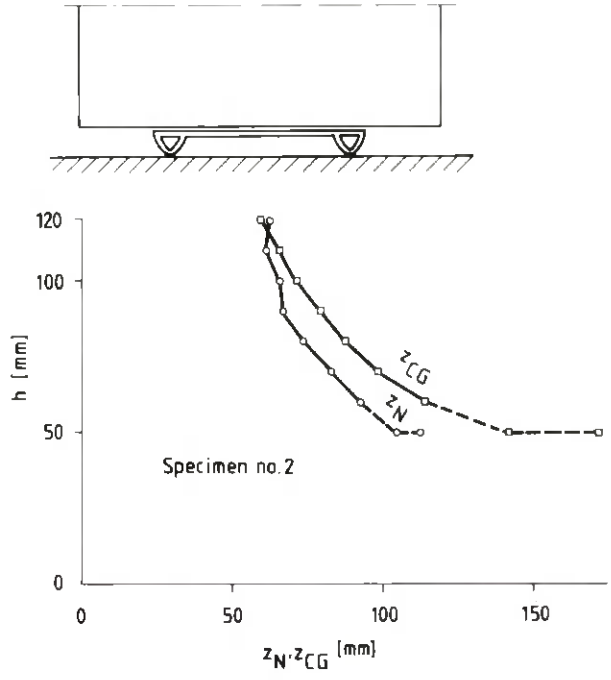

Figure 2.12 b.

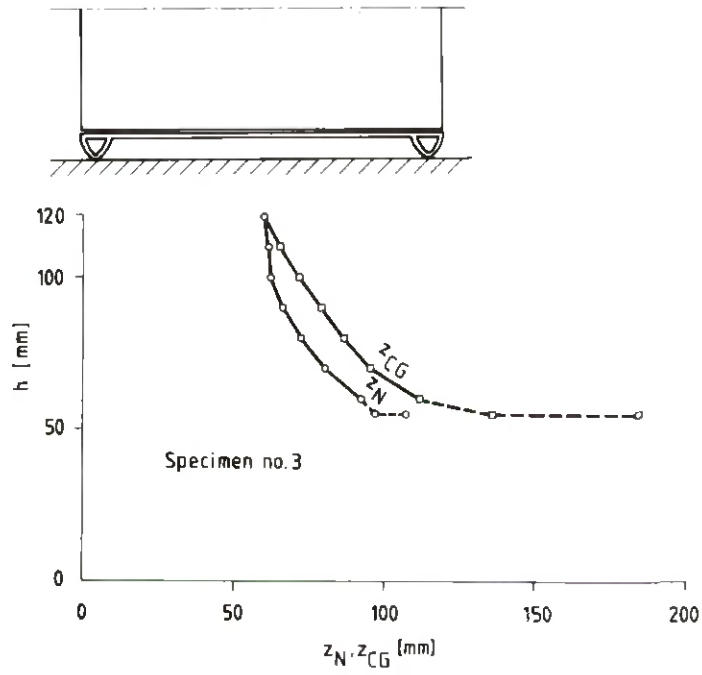

Figure 2.12 c.

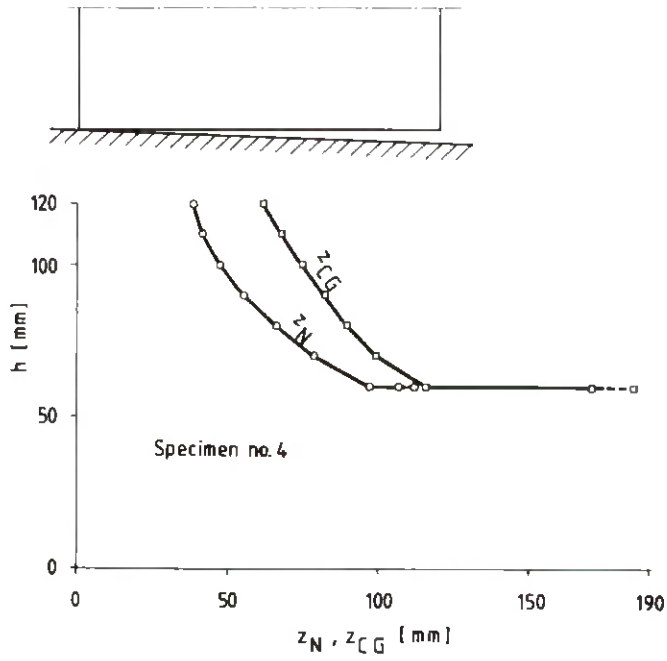

Figure 2.12 d.

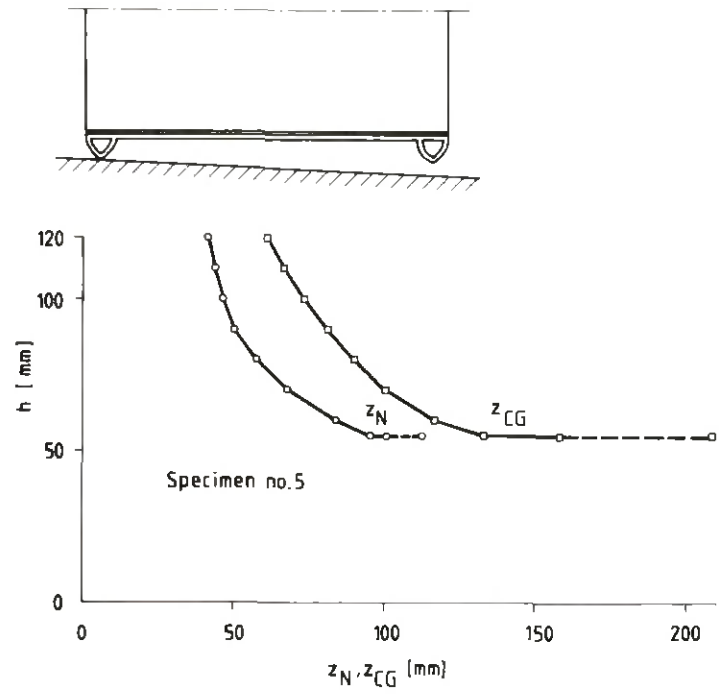

Figure 2.12 e.

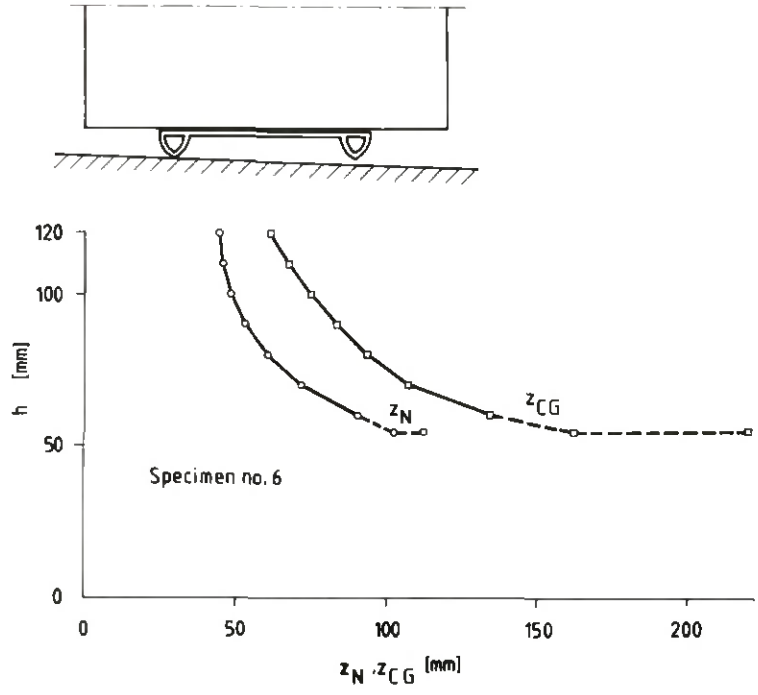

Figure 2.12 f.

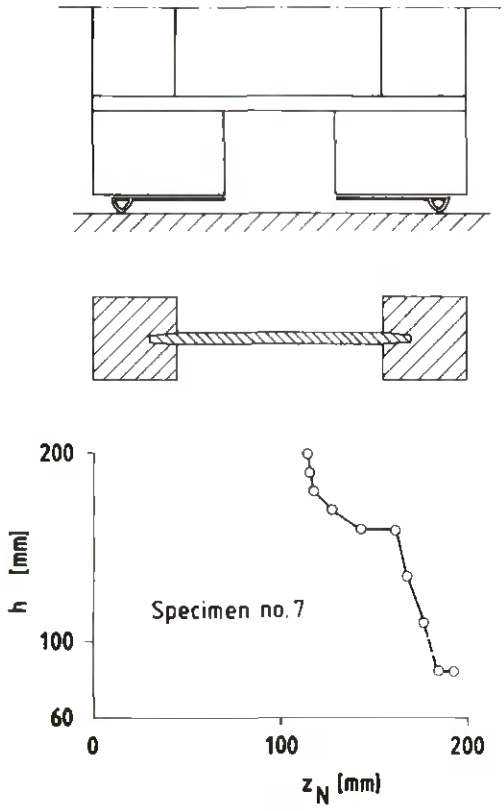

Figure 2.12 g.

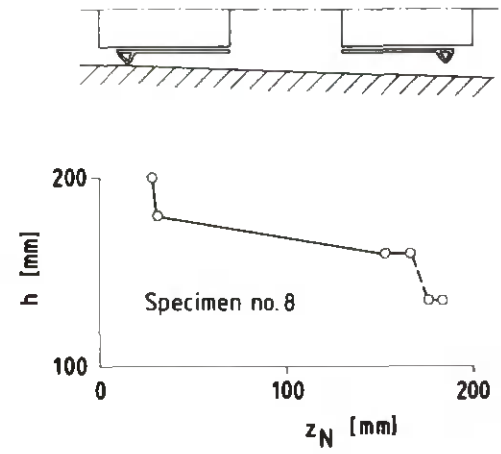

Figure 2.12 h.

The diagrams show that the position of the axial force for the whole cross section is dependent on support conditions. For a horizontal base plate, the load was very near the centre in the cases where rubber strips were used (specimens Nos. 2 and 3), while in specimen No. 1 where the stiffness properties of the sole plate exerted a large influence it had a more eccentric position. In tests with an inclined base plate, the eccentricity of the load was considerable but fairly independent of the other support conditions.

Displacement of the position of the axial load during application of the load is shown in Figure 2.13 for the last cross sectional stage of the specimens. Specimen No. 8 is not included since the cause of failure was reduction in strength of the web near the bottom support. See below.

For specimen No. 4, in which creep proceeded for 2 hours before failure occurred, the position of the axial load and the geometrical centroid of the cross section are also plotted as a function of the time, measured from the time when the maximum load was applied. See Figure 2.14.

In the lightweight studs, specimens Nos. 7 and 8, obvious buckles were noted in the web after one flange had been removed and the web thus had an unsupported edge. After further reduction of the cross section there were no more visible buckles since the slenderness ratio of the web decreased. At the final stage of the test, collapse was initiated by compressive failure in the web.

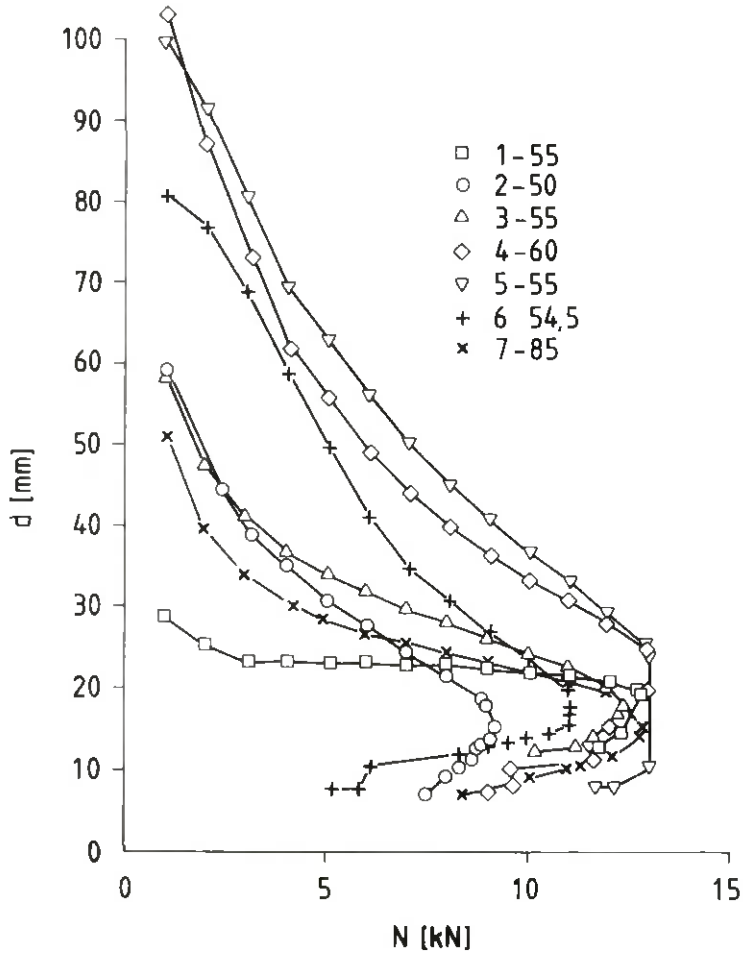

Figure 2.13. Position of the axial force as a function of load for the smallest cross sections in the tests.

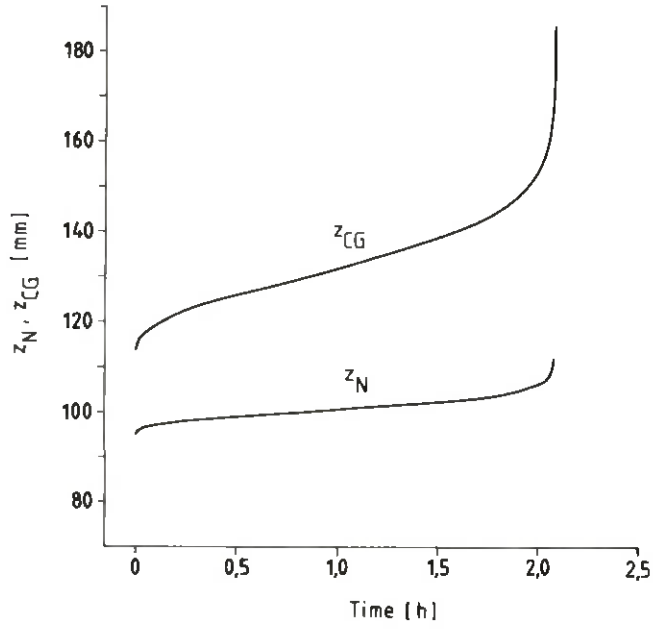

Figure 2.14. Creep prior to failure in specimen No. 4. Position of the axial force and the geometrical centre of gravity of the beam cross section as a function of time from the application of the maximum load.

The web butt joint in specimen No 8 which was placed 260 mm from the bottom end of the stud had a considerable influence on deformational behaviour, and this was further accentuated because of the inclination of the base plate. When 40 mm of one of the flanges had been removed by planing, the web was no longer capable of transmitting the load to the other whole flange which was not in contact with the inclined base plate initially. Deformations however became so large that the entire flange was soon forced against the base plate, and the axial load had moved to the flange. After the last pieces of the flange had been removed, the axial load was in approximately the same position as for specimen No 7, see Figure 2.12 g and h. However, due to local weakening at the web butt joint, the cross section could not be reduced to the same extent as in specimen No 7.

2.4 Evaluation

2.41 Bending stiffness

In the test under transverse loading deflection was recorded at the midpoint of the beam and at a further four points, see Figure 2.4. With the aid of these displacements, the bending stiffness can be determined as the mean value over the gauge lengths ℓ_1 = 600 mm and ℓ_2 = 2000 mm. Over the gauge lengths ℓ_1, the bending moment is constant. We thus have

$$E_1 = \frac{M_0 \ell_1^2}{8 I w_1}$$

where w_1 is the rise of the elastic line over the gauge length ℓ_1.

Over the gauge length ℓ_2 the bending moment varies. With the aid of the energy equation applied to the moment distributions in Figure 2.15, we have

$$E_2 = 14.67 \cdot 10^{-3} \frac{P \ell_2^3}{I w_2}$$

where w_2 is the rise of the elastic line over the gauge length ℓ_2.

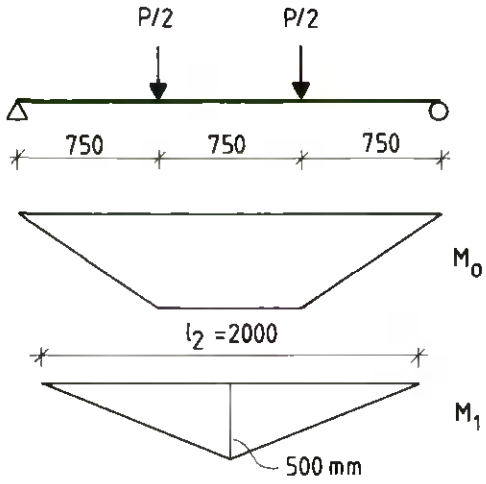

Figure 2.15.
Moment diagrams for determination of the mean flexural rigidity $(EI)_2$ over the gauge length ℓ_2.

The moduli of elasticity were determined for both gauge lengths and for all stages of the cross section in specimens of Type 1. The values were found to have no appreciable dependence on the depth h of the cross section.

The variations which did occur were largely due to measuring errors caused by the limited accuracy of readings by the load cells. Only the mean values of the moduli of elasticity and the standard deviations are therefore set out for each specimen in Table 2.5. The scatter in the values of E_1 is greater than in the case of E_2, since the incidence and position of defects had a greater influence over the shorter gauge length ℓ_1.

In the case of specimens Nos. 7 and 8 it was found that the load level had been too low and the load values far too unreliable for values of the flexural rigidity to be given for the specimens.

Table 2.5. Results from determination of the moduli of elasticity for the gauge lengths ℓ_1 = 600 mm and ℓ_2 = 2000 mm, and associated standard deviations.

Specimen	E_1 N/mm^2	s_1 N/mm^2	E_2 N/mm^2	s_2 N/mm^2
1	9117	767	10751	339
2	14270	1173	9107	268
3	17033	1567	10425	361
4	13664	2415	9085	341
5	17777	1797	12313	413
6	16881	2015	11056	614

2.42 Stresses at midsection at failure

Once the position of the axial force and midpoint deflections of the stud are known, it is possible to calculate the maximum extreme fibre stresses σ_{mc} and σ_{mt} at the midsection. This was done for specimens Nos. 1, 4, 5, 6 for loads very near the ultimate load N_u, i.e. when the flat portion of the curve had been reached, and for specimens Nos. 2 and 3 for the ultimate load N_u where the curve exhibited a more or less pronounced maximum. See Figure 2.8. In the calculations, linear distribution of stress over the cross section was assumed. The axial force was assumed to be at the same position at both supports. The errors which arise in this way are likely to be small since the measured distances of the load from the edge exhibit fairly small variations in the vicinity of the ultimate load and are considerably less than the midpoint displacements of the stud, see Figure 2.11. The results of calculations are set out in Table 2.6.

The calculated compressive stresses σ_{mc} are at a level to be expected when the characteristic value of compressive strength is 15 N/mm^2. It is

obvious that failure commenced on the compression sides of the studs. Owing to the plastic deformations on the compression side near failure, tensile stresses also rose rapidly, which explains why a crack also occurred at failure at a knot on the tensile side near the midsection.

Table 2.6. Extreme fibre stresses at midsection near failure calculated with the aid of measured values of the eccentricity.

Specimen	N kN	e mm	σ_{mc} N/mm^2	σ_{mt} N/mm^2
1	12,70[a)]	19,7[a)]	16,2	5,9
2	9,22	38,0	22,8	14,6
3	12,36	34,1	23,6	13,6
4	12,97	19,4	14,1-32,4[b)]	4,5-22,7[b)]
5	12,93	35,3	25,3-34,9[b)]	14,9-24,4[b)]
6	10,96	51,3	29,7	20,8

a) Value somewhat too low since the stroke of the displacement transducer had been exceeded.

b) The values relate to the beginning and end of the creep stage at a constant load level.

3. ANALYTICAL MODELS

3.1 Member with pin jointed end supports in compression

The stud is assumed to be pin jointed at the ends. The Euler buckling load can be calculated with the aid of the moduli of elasticity determined in the bending tests. The value E_2 for the gauge length ℓ_2 = 2000 mm is more relevant for buckling, and this is therefore used in the calculations. The Euler buckling load is thus

$$N_E = \frac{\pi^2 E_2 I}{\ell_k^2} \qquad (3.1)$$

where ℓ_k = 2490 mm.

The results for the cross sections at failure for specimens Nos. 1-6 are set out in Table 3.1 and are compared with the ultimate loads N_u obtained in the tests. In all cases, the calculated critical load was exceeded in the tests. It therefore follows that the assumption of pin jointed end supports is very conservative. In actual fact, the critical axial force should considerably exceed the ultimate load since there is no pure buckling case in these circumstances.

Table 3.1. Comparison of the values of critical axial force calculated for studs with pin jointed ends and experimental ultimate loads.

Specimen	h mm	N_E N	N_u N	$\frac{N_u}{N_E}$
1	55	10677	12800	1,20
2	50	6795	9220	1,35
3	55	10354	12360	1,20
4	60	11714	13000	1,11
5	55	12229	13000	1,06
6	54,5	10684	11070	1,04

Owing to the imperfections of the stud etc, the design compressive force N_{cd} is lower than the Euler load N_E. The design loadbearing capacity is determined as

$$N_{cd} = k_c f_c bh$$

According to the CIB Code /4/, k_c can be calculated as

$$k_c = 0.5[(1 + (1 + \eta\lambda \frac{f_c}{f_m})k_E) - \sqrt{(1 + (1 + \eta\lambda \frac{f_c}{f_m})k_E)^2 - 4k_E}]$$

where $k_E = \frac{\sigma_E}{f_c} = \frac{\pi^2 E_0}{f_c \lambda^2}$

λ = slenderness ratio = ℓ_k/i
i = radius of gyration
σ_E = Euler buckling stress
f_c = compressive strength parallel to the grain
f_m = bending strength parallel to the grain

The initial curvature is expressed as

$e = \eta r \lambda$

where r = radius of the core.

The design loadbearing capacity was calculated on the basis of the following assumptions:

a) The maximum experimental compressive stresses according to Table 2.6 were used as the compressive strength parallel to the grain. For specimens Nos. 4 and 5 the value at the beginning of the creep stage was used.

b) The ratio f_c/f_m was put equal to 1.

c) The experimental values E_2 according to Table 2.5 were used as th modulus of elasticity.

d) The initial curvature is the same as the rise at the centre of the stud = $l_k/1000$. The initial curvature of the specimens was not measured, but since they were very straight, the value chosen is a reasonable assumption.

The results of calculations are set out in Table 3.2.

Table 3.2. Comparison of the design loadbearing capacity N_{cd} calculated according to /4/ and the experimental ultimate loads N_u.

Specimen	N_{cd} kN	$\frac{N_{u,exp}}{N_{cd}}$
1	9746	1,313
2	6501	1,418
3	9788	1,263
4	10590	1,228
5	11483	1,132
6	10206	1,085

3.2 Member with cylindrical convex end surfaces in compression

3.21 Critical load

During the tests it was noted that the ends of the studs not only rotated but also performed a rolling motion like a wheel. In order that this mechanism may be described in a simple manner, it may be assumed that the end surfaces of the stud or the surfaces of the base are convex and cylindrical, see Figure 3.1. The way this idealisation is carried out is described in Subsection 3.23.

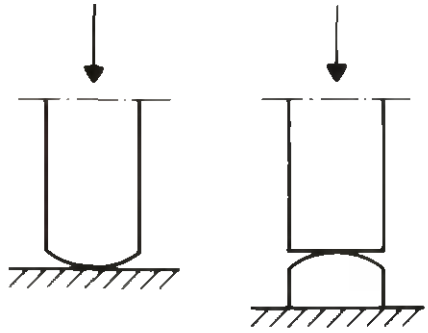

Figur 3.1. Convex cylindrical contact surfaces at the end support of the member.

As an anlysis of a stud in compression, of such a shape, is carried out in Appendices A1-A3. The critical axial force, i.e. the bifurcation load or Euler load N_E, is calculated as

$$N_E = \frac{\pi^2 EI}{\ell_k^2}$$

The effective length $\ell_k = \beta\ell$ is dependent on the radius r of the contact surface and is given in Figure A3. The length of the member is ℓ, see Figure A1. It is evident that there are two limiting cases. The first occurs when r = 0 and corresponds to Euler Case 2, with pinjointed ends and an effective length $\ell_k = \ell$. The other extreme case implies that r = ∞ and corresponds to Euler Case 4, with fixed ends and the effective length $\ell_k = \ell/2$.

3.22 Eccentric compressive force

During stages of the cross section which occur when the member chars due to exposure to fire on one side, loading is eccentric with an eccentricity a with respect to the remaining cross section. See Figure A4. The section properties of the member can be calculated when its deflection is known. Applying second order theory, see Appendix A2, the deflection at the midpoint is

$$v(\frac{\ell}{2}) = v_{max} = a[1 - \frac{r\alpha \tan \frac{\alpha\ell}{2}}{1 + r\alpha \tan \frac{\alpha\ell}{2}}] (\frac{1}{\cos \frac{\alpha\ell}{2}} - 1) \qquad (3.2)$$

and the rotation at the end of the member is

$$v'(0) = \frac{\alpha a \tan \frac{\alpha\ell}{2}}{1 + r\alpha \tan \frac{\alpha\ell}{2}} \qquad (3.3)$$

where $\alpha = \sqrt{\frac{N}{EI}}$

For an inclined support, see Figure A6, there is a load eccentricity of magnitude θr where θ is the magnitude of the inclination. The same formulae as above can thus be used, the eccentricuty being replaced by θr.

3.23 Determination of the ideal radius of the stud's end surfaces

In actual fact, the shape of the support of the stud is different from the idealised assumption that the end surface is cylindrical. With the aid of the experimental relationships between axial force and midpoint deflection, see Figure 2.7, and the theoretical expression for v_{max} in Equation (3.2), calculations were made of the radii r_i of the contact surface as a function of v_{max} which satisfies the condition

$$v_{max}^{calculated} = v_{max}^{experimental}$$

i.e. that geometrical shape of the end surfaces of the stud was calculated which would have produced the same deflection of the stud as that obtained in the tests.

In the calculations the initial curvature of the stud was ignored since the specimens were very straight. The eccentricity was thus

$$a = \frac{h_o - h}{2} + \theta r_i$$

Since specimens Nos. 4-6 had an inclined support at the bottom of the stud and a horizontal support at the upper end, the approximate value $\theta = 0.0175$ was used, i.e. the mean value of the two support inclinations.

The results of this analysis are set out in Figure 3.2 a-f. It is a common characteristic of specimens Nos. 1-3 that the radius r_i assumes very large values for small deflections. For specimens Nos. 4-6 the radius does not assume very large values until the midpoint deflection is between 11 and 16 mm. At this point the rotation $v'(0)$ of the end of the member is approximately 0.0175, i.e. the same as the mean value of the inclinations of the support plates. After this the radius continues to decrease, and at the same time the midpoint deflection v_{max} increases. This characteristic shape of the curves is particularly pronounced in specimens Nos. 1, 3, 4 and

5, i.e. the ones which were fitted with 120 mm wide rubber sealing strips or had no strips at all. In specimens Nos. 2 and 6 which had the narrower, only 70 mm wide rubber profiles, the curves in some cases had a maximum which was however clearly different from the high values obtain for the other specimens.

At this stage the stud was "balancing" on the narrow rubber profile. For very large deflections, the curves for all specimens exhibit approximately the same values of the ideal radius. In this position, even in the case of specimens Nos. 2 and 6, the end of the stud had rotated so much that good contact had been obtained between the end of the sole plate and the end plate. This evaluation of the test results was not carried out for specimens Nos. 7 and 8 since their bending stiffness was not determined with sufficient accuracy. See Subsection 2.41.

In some cases, small ideal radii were calculated for small midpoint deflections v_{max}. The probable reason for this is that the small axial force was not enough to compress the rubber seal sufficiently. See the results for specimens Nos. 1 and 2 in Figure 3.2a and 3.2c.

The experimental relationships between the ideal radius and the midpoint deflection, calculated with the aid of the analytical model, exhibit the same characteristic shape. Particularly for large values of v_{max}, the differences between the different curves representing the last cross sectional stage are fairly small.

Figure 3.2 a-f. Ideal radius - midpoint deflection curves for the studs.

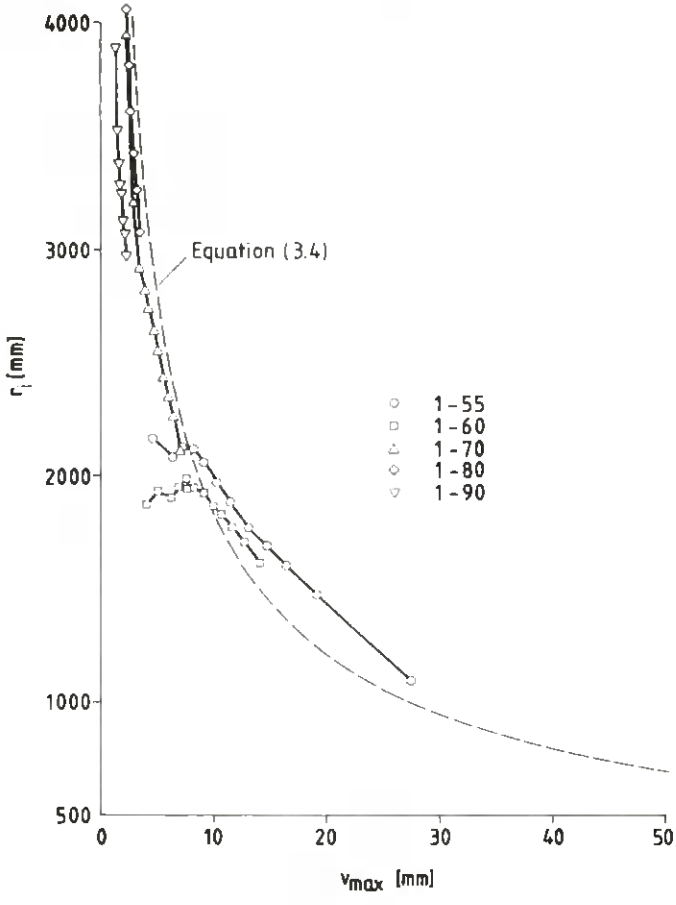

Figure 3.2. a

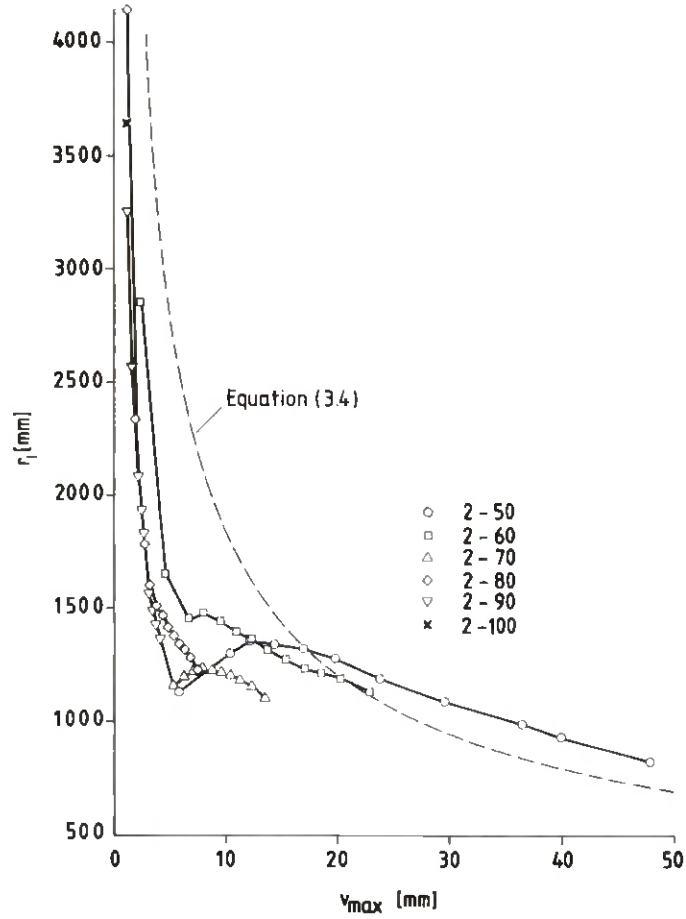

Figure 3.2. b

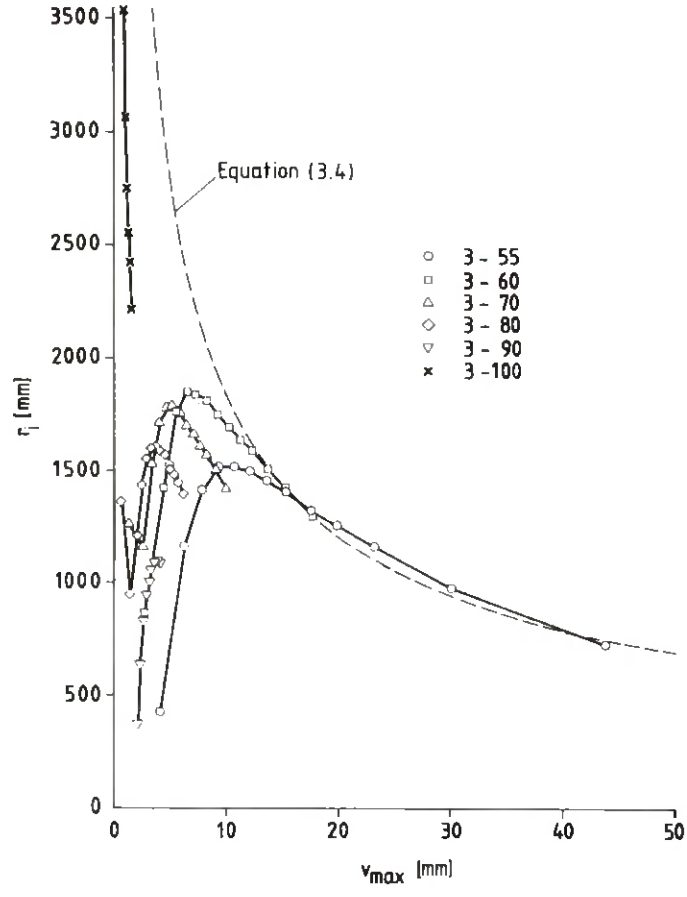

Figure 3.2. c

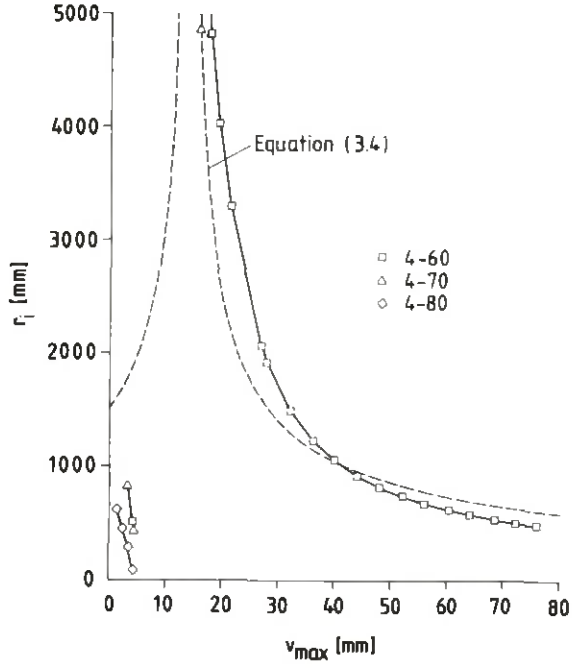

Figure 3.2. d

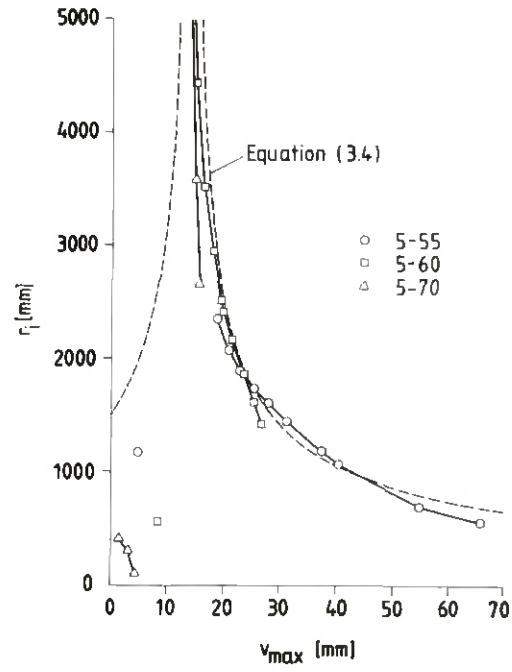

Figure 3.2. e

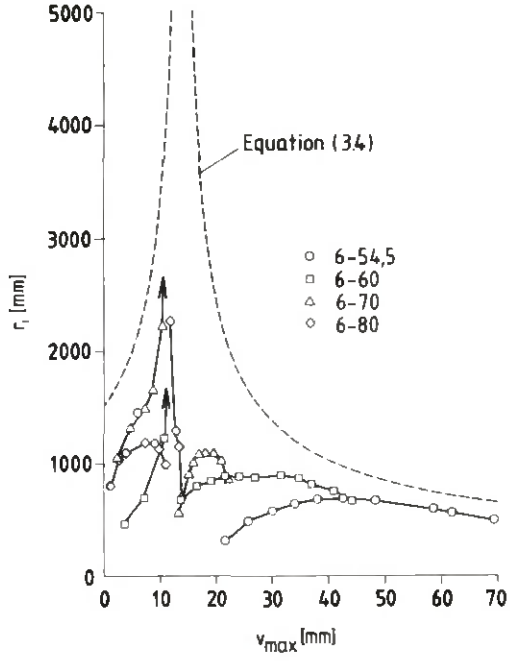

Figure 3.2. f

In order that these curves may be used in calculating the loadbearing capacity, an approximate expression was determined for the ideal radius by curve fitting. Particular attention was paid to values in the vicinity of the ultimate stage. The proposed expression is

$$r_i = \frac{7300}{|(v_{max} - 793\ \theta)|^{0,6}} \qquad (3.4)$$

where v_{max} and r_i are in mm.

In the formula, the inclination of the support is taken into consideration by utilising the relationship between the rotation at the end support and the midpoint deflection for an assumed sinusoidal elastic line. The deflection is then described as (see Figure A1)

$$v = v_{max} \sin\frac{\pi}{\ell} x$$

and the rotation at the end support is

$$v'(0) = \frac{\pi}{\ell} v_{max}$$

Thus $v_{max} = v'(0) \frac{\ell}{\pi}$

With ℓ = 2490 mm, we have

$$v_{max} = 793\ v'(0) \qquad (3.5)$$

Expression (3.4) for the ideal radius is plotted with dashed lines in Figure 3.2 a-f.

With the aid of the approximate expression (3.4) for the ideal radius, the theoretical relationship between the axial force and the midpoint deflection, and the theoretical ultimate load, was then determined for specimens Nos. 1-6. The theoretical ultimate load is defined as the load at which the maximum compressive stress at the centre of the member is equal to the experimental values σ_{mc} set out in Table 2.6. In the calculations, the moduli of elasticity E_2 according to Table 2.5 were used.

Since the ideal radius is dependent on deflection (in actual fact it is dependent on end rotation), the correct ideal radius is calculated by iteration. After choosing an initial value for r_i, v_{max} is calculated according to (3.2), whereupon a new value of r_i is determined according to (3.4), and the procedure is repeated until there is good agreement between the new and old value of r_i.

The results of these calculations are set out in Figure 3.3 a-f and in Table 3.3 where the values of the critical load N_E and the theoretical ultimate load $N_{u,theor}$ are tabulated. The latter is also marked on the appropriate theoretical load-deflection curve. The critical load N_E is calculated for the same ideal radius which occurs when the load is equal to the ultimate load.

The agreement between the experimental and calculated load-deflection curves is good for specimens Nos. 1-3 and 5, and less good for specimens Nos. 4 and 6. It was only in the case of specimen No. 6, for which the narrow, only 70 mm wide, rubber profile had been used, that values which were obviously on the unsafe side were obtained.

Figure 3.3 a-f. Calculated and experimental load-deflection curves. The ultimate load according to Table 3.3 is marked on the theoretical curve.

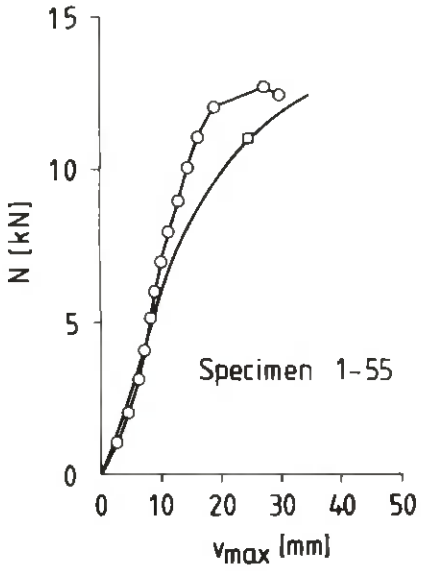

Figure 3.3. a

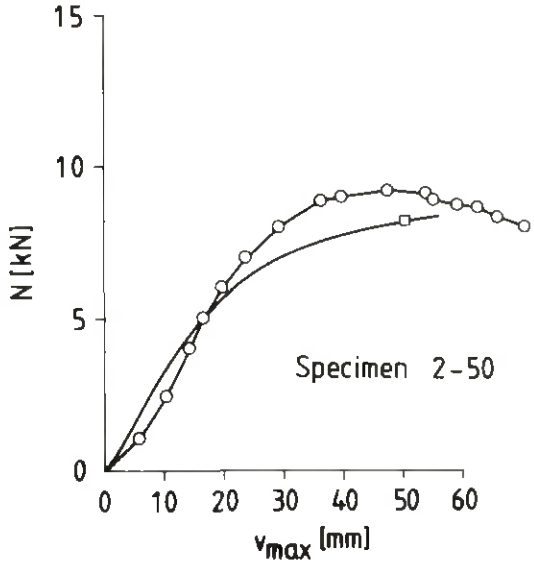

Figure 3.3. b

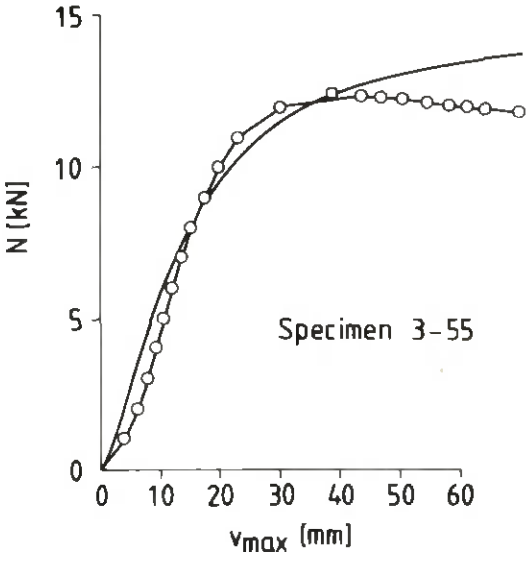

Figure 3.3. c

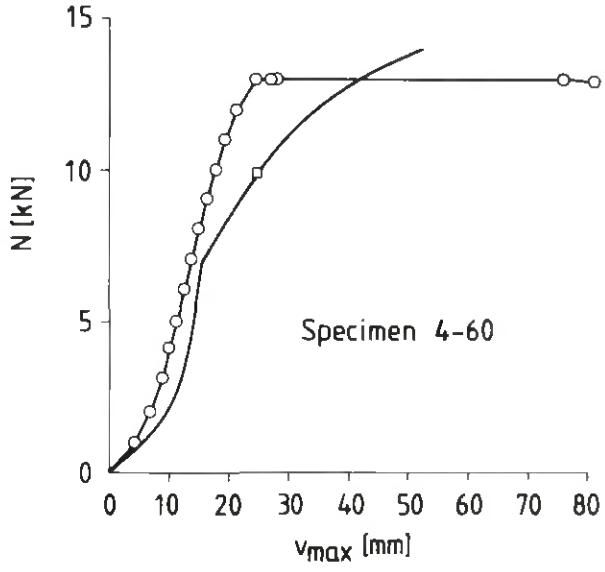

Figure 3.3. d

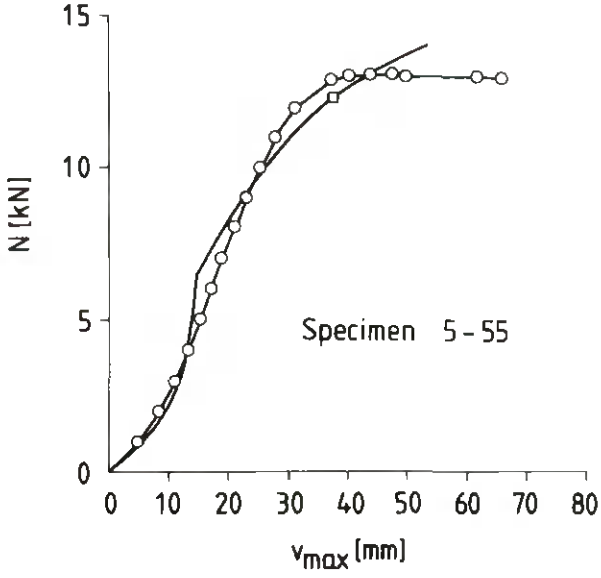

Figure 3.3. e

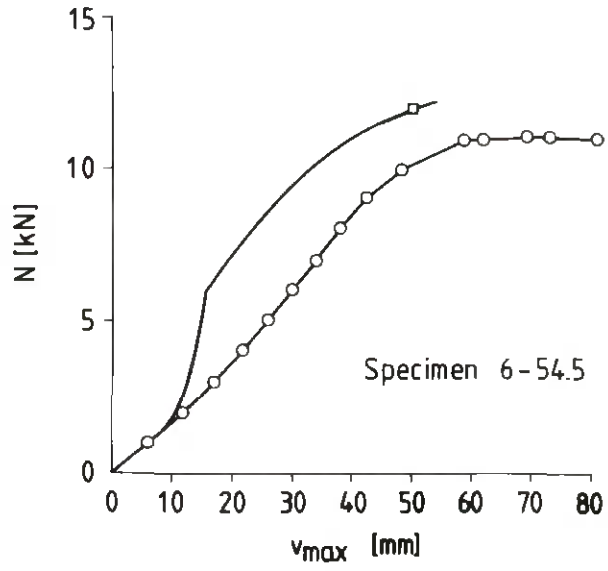

Figure 3.3. f

Table 3.3. Comparison of calculated and experimental ultimate loads according to the analytical model "member with cylindrical end surfaces".

Specimen	h	N_E	$N_{u,exp}$	$N_{u,theor}$	$\frac{N_u}{N_{u,theor}}$	$\frac{N_{u,theor}}{N_E}$
	mm	kN	kN	kN		
1	55	32416	10974	12800	1,157	0,339
2	50	17528	8177	9220	1,128	0,467
3	55	28575	12428	12360	0,995	0,435
4	60	39900	9915	13000	1,308	0,325
5	55	37441	12295	13000	1,052	0,345
6	54,5	29950	11975	11070	0,915	0,366

3.24 The influence of the stud cross section

Owing to rotation of the stud at the support, the point of contact with the support, i.e. the position of the axial force, is increasingly displaced towards one of the edges. At the opposite edge an increasingly wide gap is formed between the end surface of the stud and the base, and at ultimate stage this gap may extend as far as the middle of the cross section, see Figure 2.9 and 2.10. This means that the internal forces of the stud at this stage are independent of the original depth of cross section, and that Equation (3.4) can be used also when the original depth is different from 120 mm.

3.25 The influence of the length of the stud

Expression (3.4) for the ideal radius was determined for the stud length ℓ = 2490 mm. In order that this formula may be used for other stud lengths, it must be modified.

For a member with rounded ends, the instantaneous radius which holds for a certain load is dependent only on the end rotation v'(0). When two members (1) and (2) of lengths ℓ_1 and ℓ_2 respectively have the same end rotation v'(0), see Figure 3.4, we have the following relationship when the deflection curves v(x) are affine:

$$\frac{v_{max1}}{v_{max2}} = \frac{\ell_1}{\ell_2}$$

When the ideal radius is expressed as a function of v_{max}, as in Equation (3.4), v_{max} is multiplied by the term $\ell/2490$ where ℓ is the actual stud length in mm. Inclination of the support is taken into consideration by multiplying it by ℓ/π.

We thus have:

$$r_i = \frac{7300}{\left|\left(v_{max}\,\frac{\ell}{2490} - \frac{\ell}{\pi}\,\theta\right)\right|^{0,6}} \qquad (3.8)$$

If the ideal radius is expressed as a function of the end rotation v'(0), a correction with respect to different stud lengths is not necessary.

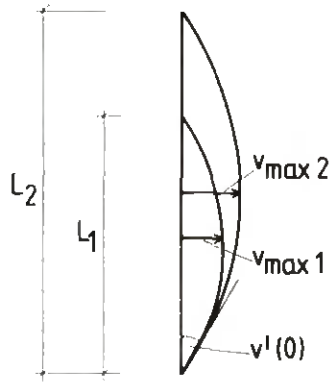

Figure 3.4.
Maximum deflections of members of different lenghths for affine deflection curves.

3.26 The influence of support inclination on loadbearing capacity

In order to elucidate the influence of support inclination on the loadbearing capacity, the ultimate load was calculated for a stud of the dimensions and material values corresponding to those of specimen No. 6-54.5. The ultimate load was calculated for different support inclinations θ and is plotted in Figure 3.5 in relation to the ultimate load at $\theta = 0$. The maximum compressive stress $\sigma_{mc} = 29,7\ N/mm^2$ was used as the failure criterion.

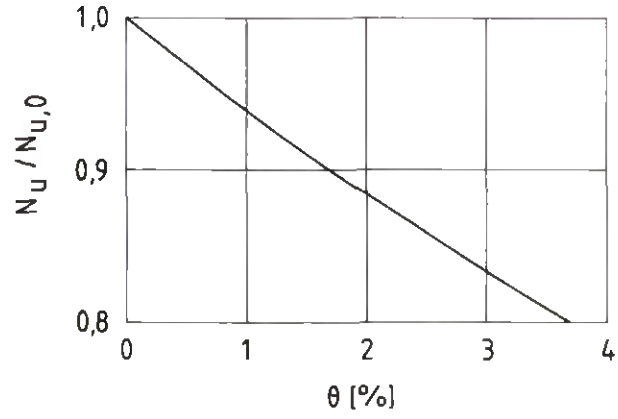

Figure 3.5. The influence of the inclination of the support plates on the ultimate load of a wall stud with the cross sectional and material data according to specimen No. 6-54.5.

The support may have an inclination for a number of reasons. It is probable, however, that lack of dimensional accuracy in the timber can be excluded as one of these. Most studs are at present cut with a saw on a bench. It is only in exceptional cases that the timber is cut by hand and there is a risk of unintentional skew cutting. Since sole plates are also planed, they have very good accuracy. On the other hand, irregularities in the concrete slab or a deviation in its surface from the horizontal may give rise to support inclination. The aim in modern building is to avoid such defects. Concrete floors are given intentional slopes only in the vicinity of floor gulleys. With studs spaced at 600 mm, it is possible for two adjacent studs to be situated in such an area. However, such an inclination has no unfavourable effect on the loadbearing capacity of the external wall in the event of fire, since the base is inclined towards the building on the side epxosed to fire. In the case of core walls, however, the floor gulley may be placed on the side which is not exposed to fire, and in such a case it may have an unfavourable effect.

A typical value for the support inclinations which are possible in practice due to the deflections of roof trusses can be given with regard to the fact that these are often limited to L/300 where L is the span of the truss. Such a deflection implies that the rotation of the rafter of the truss is $\theta \approx 0.013$ at its end support. If the bottom support is horizontal, then the stud can be approximately replaced by one whose both supports have the inclination $\theta = 0.065$. According to Figure 3.5, the ratio $N_u/N_{u,0} \approx 0.96$, i.e. the influence of the support inclination is very small.

3.27 Superposition of axial force and transverse loading

An analysis of a wall stud with cylindrical convex end surfaces, which is acted upon by both axial and transverse loading, is carried out in Appendix A4. The aim of this analysis was to find how these two loading cases are to be superimposed. This is of importance when both loading cases are studied individually by experiments.

The interaction formula

$$\frac{N}{N_d} + \frac{M}{M_d} = k \qquad (3.10)$$

was determined for a wall stud of a shape equal to specimen No 2-50 and for the design compressive strength f_c = 15 N/mm^2. N_d and M_d are the design values for only compressive and transverse loading respectively. In an unfavourable case the interaction curve may have the appearance as in Figure 3.6 where the ideal radius r_i had been determined according to (3.4). The deviation from the linear relationship with k = 1 is very small.

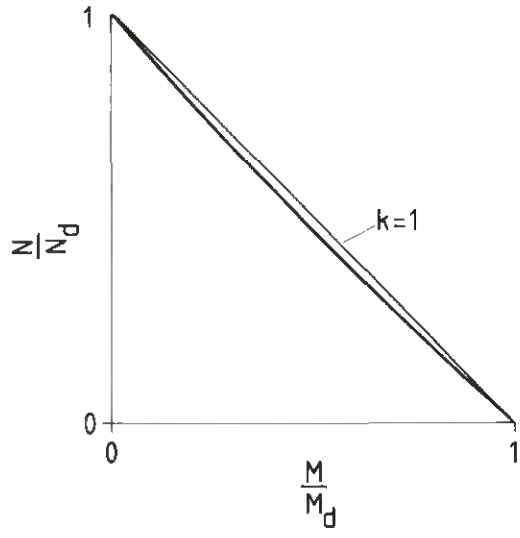

Figure 3.6. Interaction curve for compressive force N and bending moment M due to transverse load. The failure criterion is the compressive strength f_c. The geometrical shape is the same as for specimen No 2-50.

The least value of k occurs for M/M_d = 0.5. In order to find in what way k_{min} depends on the susceptibility to buckling of the stud, a parametric study was carried out. Since the slenderness ratio ℓ_k/i of the stud is dependent on the ideal radius, and since this is usually different for determination of M_d and N_d, the compressive strength f_c was varied instead. The quantity k_{min} is shown as a function of the ratio E/f_c. This study was made on the assumption that the ideal radius is constant and

equal to 1000 mm, and the assumption that the ideal radius varies according to Equation (3.4). The results of this parametric study are given in Figure 3.7. Small values of E/f_c imply that the compressive force is near the critical compressive force N_E.

The results for k_{min} show that k in (3.10) can be approximately put equal to 1. The interaction relationship is thus

$$\frac{N}{N_d} + \frac{M}{M_d} = 1 \qquad (3.11)$$

and may produce results which are a little on the unsafe side.

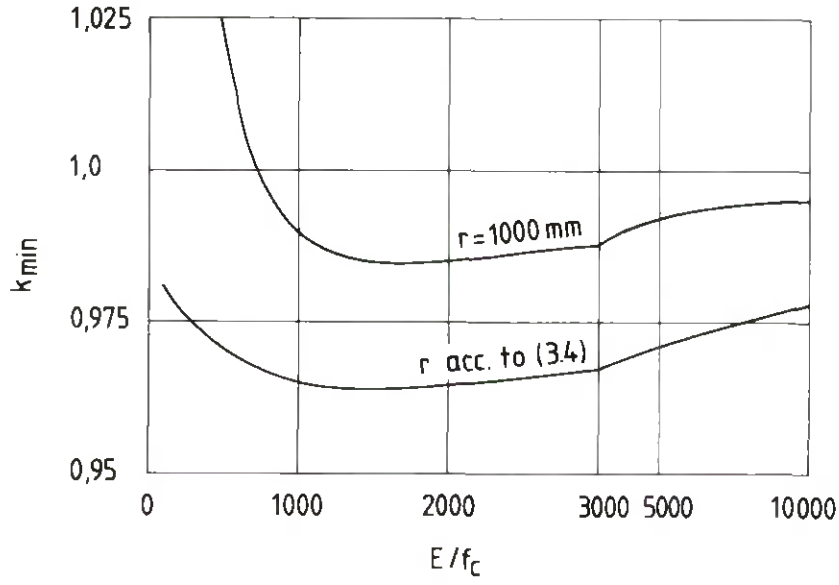

Figure 3.7. Relationship between k_{min} and the quantity E/f_c. Cross sectional data and modulus of elasticity as for specimen No 2-50.

4. CONCLUSIONS

The previous chapter describes an investigation of the applicability of two analytical models for the description of the structural behaviour of axially loaded studs subject to the action of fire on one side.

The analytical model discussed in Section 3.1 in which the ends of the studs are assumed to be pin jointed considerably underestimates the load-bearing capacity. It is only for the specimens with very large support inclinations that there is better agreement between the theoretical and experimental ultimate loads. The assumption concerning pinjointed supports which is unfavourable for the loadbearing capacity is to some extent compensated for by the unfavourable influence of the support inclination.

The second analytical model treated in section 3.2 describes the structural behaviour considerably better. The stud is assumed to be placed between rigid end plates and the end surfaces of the stud area assumed to be convex and cylindrical. Even though the experimental basis for determination of the ideal radius of the end surfaces has been of small extent, the support conditions for the different specimens showed very large differences. The studies showed that it is possible to describe the ideal radius by an approximate expression and to obtain good agreement between theoretical and experimental results. It is only in the case of specimens fitted with sealing strips which are considerably narrower than the depth of the stud that the approximate expression differs from the experimental relationships. Compared with the wide strips, these narrow rubber sealing strips represent a point of weakness. When the rubber sealing strip is of the same width as the depth of cross section, there is no significant difference between the loadbearing capacities obtained. It is possible further to improve accuracy by better curve fitting for the expression (3.4). However, in order that an expression of greater general validity may be obtained, more experiments are probably necessary.

This second analytical model provides a considerably better description of the real structural behaviour. It is therefore possible to study the effect of different parameters by calculations.

At present, the thermal effects of fire on the strength and stiffness of small cross sections is insufficiently known. For this reason, the use of only theoretical methods for determination of the loadbearing capacity in the event of fire is often far too unreliable, and fire tests are therefore unavoidable. However, tests need not comprise different support conditions such as inclined supports, since these can be dealt with separately by means of the analytical model.

The theoretical studies have shown that complete design for axial and transverse loading can be carried out by linear superposition of these two loading cases.

In broad outline, the following procedure may be adopted in fire testing loadbearing timber stud walls:

- Fire tests are carried out separately for axial and transverse loads. Since the primary interest is to determine the loadbearing capacity of the construction after a certain fire resistance period, e.g. according to code requirements, the fire test is discontinued after this time. Both the axial and transverse load are maintained constant during the

entire fire test, and their magnitude is such as to ensure that failure does not occur before the stipulated time. Load is then increased until failure occurs.

The loadbearing timber stud wall can thus be designed for the loading case fire plus for any other loads from the roof (snow) or attic floor (live loads), or for loads acting perpendicular to the plane of the wall (wind loads).

REFERENCES

/1/ The loadbearing capacity of elements of structure in the event of fire. (Byggnadsdelars bärförmåga vid brand). (In Swedish). Code of Statutes of the Swedish Board of Physical Planning and Building, PFS 1984:1, SBN Approval Rules, Stockholm 1984.

/2/ SBN 1980, Code of Statutes of the Swedish Board of Physical Planning and Building, PFS 1980:1, Swedish Building Code, Chapter 27 Timber Structures, Stockholm 1980.

/3/ Norén, J. & Östman, B.: The contribution of board materials to fire resistance. (Skivmaterials bidrag till brandmotståndet). (In Swedish). TräteknikRapport No 79, Swedish Institute for Wood Technology Research, Stockholm 1985.

/4/ CIB Structural Timber Design Code. CIB Report 1983, Publication 66, Working Group W18.

APPENDIX

A1. Determination of the critical load for a member with cylindrical convex end surfaces

The member in compression is assumed to have cylindrical end surfaces and is placed between two parallel support plates. The bifurcation load is characterised by the fact that the member is in equilibrium even in the deflected position, see Figure A1. The point of application of the load has then been displaced somewhat in the direction of deflection, see Figure A2.

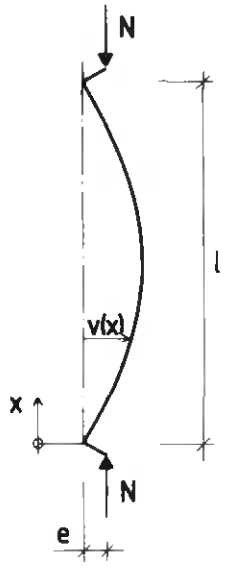

Figure A1.
Member in deflected equilibrium position.

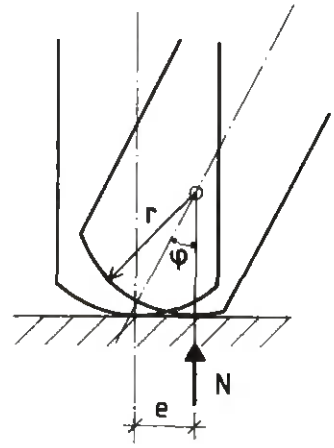

Figure A2.
Eccentricity for loaded member in the deflected position.

For small deformations, the eccentricity of the load is

$$e \approx \varphi\, r \approx v'(0)\, r$$

The bending moment on the member is then

$$M(x) = N\,[v(x) - v'(0)\, r] \qquad (1)$$

With $v''(x) = \frac{-M}{EI}$ we have

$$v'' + \frac{N}{EI}\, v = \frac{N}{EI}\, v'(0)\, r$$

With $\alpha^2 = \frac{N}{EI}$

the differential equation of the instability problem is

$$v'' + \alpha^2 v = \alpha^2 v'(0)\, r \qquad (3)$$

The general solution is of the form

$$v(x) = C_1 \sin \alpha x + C_2 \cos \alpha x + v'(0)\, r$$

Thus

$$v'(x) = C_1\, \alpha \cos \alpha x - C_2\, \alpha \sin \alpha x$$

From the boundary conditions $v(0) = 0$ and $v'(\frac{\ell}{2}) = 0$, we have

$$C_2 = -v'(0)\, r$$

and $C_1 = -v'(0)\, r \tan \frac{\alpha \ell}{2}$

The solution of the differential equation is then

$$v(x) = -v'(0)\, r \tan \frac{\alpha \ell}{2} \sin \alpha x - v'(0)\, r \cos \alpha x + v'(0)\, r \qquad (4)$$

and

$$v'(x) = -v'(0)\, r\alpha \tan (\frac{\alpha \ell}{2}) \cos \alpha x + v'(0)\, r\alpha \sin \alpha x \qquad (5)$$

$$v'(0) = -v'(0)\, r\alpha \tan \frac{\alpha \ell}{2}$$

The buckling condition is thus

$$r\alpha \tan \frac{\alpha \ell}{2} = -1$$

which can be transformed into

$$\tan \frac{\alpha \ell}{2} = -\frac{1}{r\alpha}$$

and $$\tan \frac{\alpha \ell}{2} = -\frac{1}{\alpha \ell}\frac{\ell}{r} \qquad (6)$$

The roots $\alpha\ell$ of the equation are determined for different values of $\frac{\ell}{r}$. With the effective length ℓ_k expressed as

$$\ell_k = \beta \ell$$

the solution can be described as $\beta = f(r/\ell)$ as shown in Figure A3.

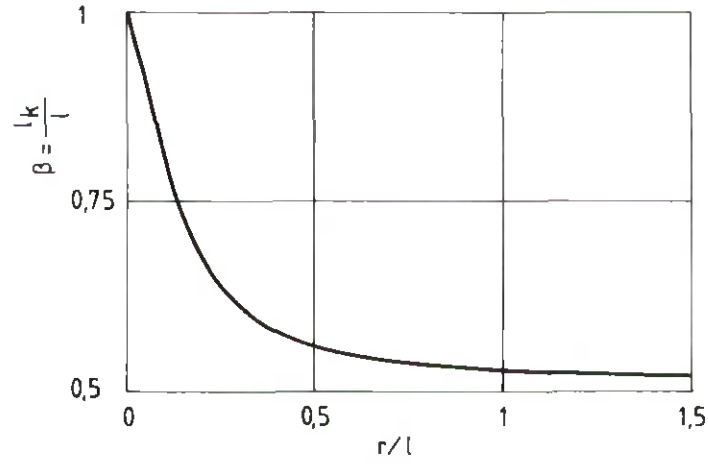

Figure A3. Effective length, expressed as $\ell_k = \beta\ell$, as a function of the end surface radius.

A member with pin jointed ends corresponds to the case r = 0. The effective length for this case is $\ell_k = \ell$, which is the effective length for Euler's second case.

The other extreme case corresponds to r = ∞, i.e. the ends of the member are plane.

In this case, the effective length is equal to $\ell/2$, which means that Euler's fourth case applies when both ends of the member are fixed.

A2. Member with cylindrical convex end surfaces acted upon by eccentric compressive load

When the ends of the member are shaped as shown i Figure A4, loading is eccentric right from the beginning. As the member deflects, the ends also rotate, and the point of application of the load is displaced in the direction of deflection.

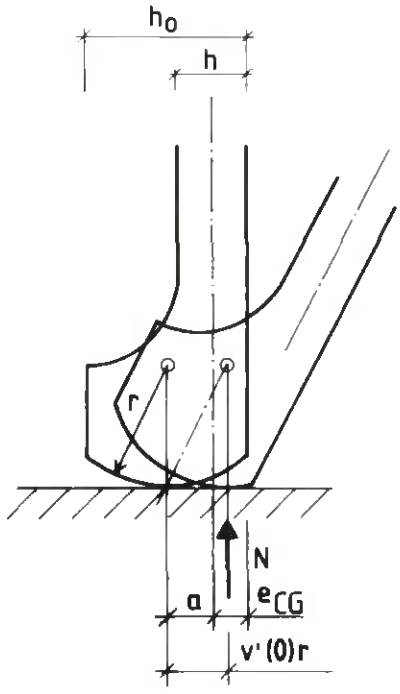

Figure A4.
Member under eccentric loading.
Point of application of load
in unloaded and loaded member.

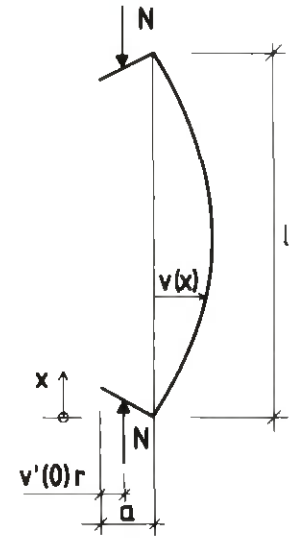

Figure A5.
Eccentrically loaded member in
deflected position.

Taking moments, we have

$$M(x) = N\,[v(x) + a - v'(0)\,r] \tag{7}$$

Substitution of $EIv'' = -M$ and $\alpha^2 = \frac{N}{EI}$ gives the differential equation of the problem

$$v'' + \alpha^2 v = \alpha^2\,[v'(0)\,r - a] \tag{8}$$

The general solution is of the form

$$v = C_1 \sin \alpha x + C_2 \cos \alpha x + v'(0)\,r - a$$

We thus have

$$v' = C_1\alpha \cos \alpha x - C_2\alpha \sin \alpha x$$

From the boundary conditions $v(0) = 0$ and $v'(\frac{\ell}{2}) = 0$, we have

$$C_2 = a - v'(0)\, r$$

and $C_1 = [a - v'(0)\, r] \tan \frac{\alpha\ell}{2}$

The solution of the differential equation is then

$$v = [a - v'(0)\, r] \tan \frac{\alpha\ell}{2} \sin \alpha x + [a - v'(0)\, r] \cos \alpha x + v'(0)\, r - a$$

and, after rearrangement,

$$v = [a - v'(0)\, r] (\tan \frac{\alpha\ell}{2} \sin \alpha x + \cos \alpha x - 1) \qquad (9)$$

In this expression, $v'(0)$ is still unknown. We have

$$v'(0) = \alpha[a - v'(0)\, r] \tan \frac{\alpha\ell}{2}$$

After some rearrangement, we have

$$v'(0) = \frac{\alpha a \tan \frac{\alpha\ell}{2}}{1 + r\alpha \tan \frac{\alpha\ell}{2}} \qquad (10)$$

Substituted into (9), this expression yields

$$v = a[1 - \frac{r\alpha \tan \frac{\alpha\ell}{2}}{1 + r\alpha \tan \frac{\alpha\ell}{2}}] (\tan \frac{\alpha\ell}{2} \sin \alpha x + \cos \alpha x - 1) \qquad (11)$$

After substitution of $x = \frac{\ell}{2}$ and some rearrangement, the midpoint deflection is obtained as

$$v(\frac{\ell}{2}) = a[1 - \frac{r\alpha \tan \frac{\alpha\ell}{2}}{1 + r\alpha \tan \frac{\alpha\ell}{2}}] (\frac{1}{\cos \frac{\alpha\ell}{2}} - 1) \qquad (12)$$

Substitution of (9) and (10) into (7) gives the moment distribution for the member. The maximum moment at the centre is obtained by substitution of (19) and (12) into (7). We thus have

$$M(\frac{\ell}{2}) = M_{max} = \frac{Na}{\cos \frac{\alpha\ell}{2}} [1 - \frac{r\alpha \tan \frac{\alpha\ell}{2}}{1 + r\alpha \tan \frac{\alpha\ell}{2}}] \qquad (13)$$

or

$$M_{max} = N a \kappa$$

where the magnification factor $\kappa = \frac{1}{\cos \frac{\alpha \ell}{2}} \left[1 - \frac{r\alpha \tan \frac{\alpha \ell}{2}}{1 + r\alpha \tan \frac{\alpha \ell}{2}}\right]$ (14)

In order that M_{max} *may be determined,* the values of $\alpha\ell$ and $r\alpha$ must be determined. We have

$$\alpha^2 \ell^2 = \frac{N}{EI} \ell^2$$

Thus $\alpha \ell = \ell \sqrt{\frac{N}{EI}}$ (15)

In addition we have

$$r\alpha = \alpha \ell \frac{r}{\ell} \quad (16)$$

There exists a stress problem for values $N < N_E$. If, on the other hand

$$N = N_E = \frac{\pi^2 EI}{\beta^2 \ell^2}$$

$M(\frac{\ell}{2})$ assumes infinitely large values, which can be easily shown by substitution.

Choose, for instance, $\frac{r}{\ell} = 0{,}25$. In Figure A3 we read $\beta \approx 1{,}64$.

Then

$$\alpha^2 = \frac{N}{EI}$$

With $N = N_E$, we have

$$\alpha^2 = \frac{\pi^2}{\beta^2 \ell^2}$$

and $\alpha \ell = \frac{\pi}{\beta}$

Thus, $\alpha \ell = \pi / 0{,}64 = 4{,}308$ och med (16)
$r\alpha = 4{,}908 \cdot 0{,}5 = 1{,}227$

Substitution of these values into (14) yields the magnification factor $\kappa = 167$. A more accurate determination of β would have resulted in a still larger magnification factor. This can be done by finding a value of $\alpha\ell$ which satisfies the buckling condition (6) a little better.

In order to calculate the maximum stresses in the member, we superimpose the stresses due to normal force and moment. In the ultimate limit state, we have

$$\frac{\sigma_c}{f_c} + \frac{\sigma_m}{f_m} = 1 \qquad (17)$$

where $\sigma_c = \frac{N}{A}$

$$\sigma_m = \frac{M_{max}}{W}$$

and f_c and f_m are the characteristic compressive and bending strengths.

A3. The influence of inclined support plates on a member with cylindrical convex end surface acted upon by a compressive force

The conditions in conjunction with an inclined support plate are illustrated in Figure A6. For small inclinations, the resultant eccentricity of load is

$$a' = \theta r$$

As the member deflects and the ends of the member consequently rotate, the point of application of the load is displaced by v'(0) r. The calculations are thus not different from the case treated in Appendix A2, and the solution given there can be applied for the load eccentricity a'.

When the support is inclined and the load is also applied with an eccentricity, the load eccentricity is increased by θr.

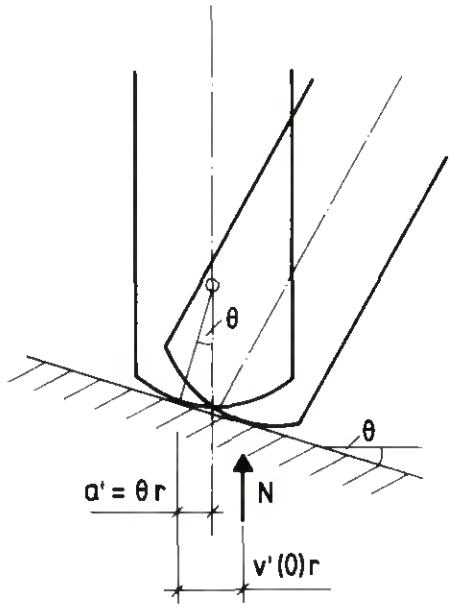

Figure A6. Eccentricity due to inclined support.

A4. Eccentric axial force and transverse load on a member with cylindrical convex end surfaces

The effect of a transverse load in addition to the eccentric axial force is studied most easily by assuming a sinusoidal moment distribution when the axial force is zero. In this case the transverse load q is also sinusoidal, see Figure A7. Taking moments for the member, we have

$$M(x) = N[v(x) + a - v'(0)\, r] + M_o \sin \frac{\pi}{\ell} x \qquad (18)$$

where M_o is the maximum bending moment due to transverse loading.

With $EIv'' = -M$ och $\alpha^2 = \frac{N}{EI}$, the differential equation of the problem is

$$v'' + \alpha^2 v = \alpha^2[v'(0)\, r - a] - \frac{M_o}{EI} \sin \frac{\pi}{\ell} x \qquad (19)$$

The particular solution has the form

$$v = C_3\, [v'(0)\, r - a] + C_4 \sin \frac{\pi}{\ell} x$$

By substitution into (19), we have

$$C_3 = 1$$

$$C_4 = - \frac{M_o}{EI(\alpha^2 - \frac{\pi^4}{\ell^2})}$$

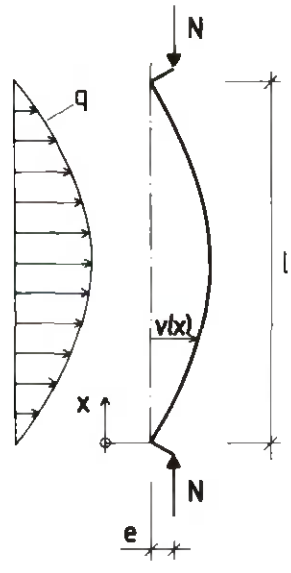

Figure A7. Member with eccentric axial force and transverse load.

The homogeneous solution is of the form

$$v = C_1 \sin \alpha x + C_2 \cos \alpha x$$

where $C_1 = [a - v'(0)\ r] \tan \frac{\alpha \ell}{2}$

$C_2 = a - v'(0)\ r$

see A2.

We have

$$v'(x) = \alpha C_1 \cos \alpha x - \alpha C_2 \sin \alpha x + \frac{\pi}{\ell} C_4 \cos \frac{\pi}{\ell} x$$

Thus

$$v'(0) = \alpha C_1 + \frac{\pi}{\ell} C_4$$

After substitution of the expressions for C_1 and C_4 and some rearrangement, we have

$$v'(0) = - \frac{\alpha a \tan \frac{\alpha \ell}{2} - \frac{\pi}{\ell} \frac{M_o}{EI\ (\alpha^2 - \frac{\pi^2}{\ell^2})}}{1 + r\alpha \tan \frac{\alpha \ell}{2}} \qquad (20)$$

The solution of the differential equation is thus

$$v = [a - v'(0)\ r]\ (\tan \frac{\alpha \ell}{2} \sin \alpha x + \cos \alpha x - 1) - \frac{M_o}{EI\ (\alpha^2 - \frac{\pi^2}{\ell^2})} \sin \frac{\pi}{\ell} x \qquad (21)$$

and the maximum deflection at the centre is obtained after some rearrangement as

$$v(\tfrac{\ell}{2}) = (a - v'(0)r)\ (\frac{1}{\cos \frac{\alpha \ell}{2}} - 1) - \frac{M_o}{EI\ (\alpha^2 - \frac{\pi^2}{\ell^2})} \qquad (22)$$

The maximum bending moment at the centre is thus

$$M_{max} = M(\tfrac{\ell}{2}) = N[v(\tfrac{\ell}{2}) + a - v'(0)\ r] + M_o \qquad (23)$$

A5. Member with initial curvature and cylindrical convex end surfaces acted upon by a compressive force

The effect of the initial curvature of the member can be determined by replacing it by the effect of an equivalent transverse load.

Assuming a sinusoidal shape of the initial curvature

$$v_o(x) = v_o(\frac{\ell}{2}) \sin\frac{\pi x}{\ell}$$

the maximum bending moment at the centre is

$$M_o = Nv_o(\frac{\ell}{2}) \qquad (24)$$

The solution given in Appendix A5 can thus be used by inserting the above expression (24) into Equations (21), (22), and (23).

Detta digitala dokument
skapades med anslag från

**Stiftelsen Nils och Dorthi
Troëdssons forskningsfond**

TräteknikCentrum
INSTITUTET FÖR TRÄTEKNISK FORSKNING

Box 5609, 114 86 STOCKHOLM
Besöksadress: Drottning Kristinas väg 67
Telefon: 08-14 53 00
Telex: 14445 tratek s
Telefax: 08-11 61 88
Huvudenhet med kansli

Åsenvägen 9, 552 58 JÖNKÖPING
Telefon: 036-12 60 41
Telefax: 036-16 87 98

931 87 SKELLEFTEÅ
Besöksadress: Bockholmsvägen 18
Telefon: 0910-652 00
Telefax: 0910-652 65
Telex: 65031 expolar s

ISSN 0283-4634